Sea ice–ocean feedbacks in the Antarctic shelf seas

Sea Ice–Ocean Feedbacks in the Antarctic Shelf Seas

R. C. FREW AND D. L. FELTHAM

Centre for Polar Observation and Modelling, Department of Meteorology, University of Reading, Reading, United Kingdom

P. R. HOLLAND

British Antarctic Survey, Cambridge, United Kingdom

A. A. PETTY

Earth System Science Interdisciplinary Center, University of Maryland, College Park, College Park, Maryland

(Manuscript received 5 November 2018, in final form 12 July 2019)

ABSTRACT

Observed changes in Antarctic sea ice are poorly understood, in part due to the complexity of its interactions with the atmosphere and ocean. A highly simplified, coupled sea ice–ocean mixed layer model has been developed to investigate the importance of sea ice–ocean feedbacks on the evolution of sea ice and the ocean mixed layer in two contrasting regions of the Antarctic continental shelf ocean: the Amundsen Sea, which has warm shelf waters, and the Weddell Sea, which has cold and saline shelf waters. Modeling studies where we deny the feedback response to surface air temperature perturbations show the importance of feedbacks on the mixed layer and ice cover in the Weddell Sea to be smaller than the sensitivity to surface atmospheric conditions. In the Amundsen Sea the effect of surface air temperature perturbations on the sea ice are opposed by changes in the entrainment of warm deep waters into the mixed layer. The net impact depends on the relative balance between changes in sea ice growth driven by surface perturbations and basal-driven melting. The changes in the entrainment of warm water in the Amundsen Sea were found to have a much larger impact on the ice volume than perturbations in the surface energy budget. This creates a net negative ice albedo feedback in the Amundsen Sea, reversing the sign of this typically positive feedback mechanism.

1. Introduction

Satellite observations have shown Antarctic sea ice to be expanding over the past four decades (Parkinson and Cavalieri 2012). Although this increasing trend is modest, it is in stark contrast to the well-documented rapid Arctic sea ice decline. The small net increase is the result of stronger, opposing regional and seasonal trends (Holland 2014), though a rapid decline in Antarctic sea ice was observed in 2016/17 (Stuecker et al. 2017; Turner et al. 2017).

There is no clear consensus for the differing Arctic and Antarctic sea ice changes in the context of global warming. Global climate models are unable to reproduce the observed trends in Antarctic sea ice, or the regional patterns (Turner et al. 2013). Warm upper-ocean biases present in the models may explain the opposing modeled and observed trends (Schneider and Deser 2018), as it influences the surface energy balance controlling sea ice growth and melt, and the strength of ice production–mixed layer entrainment feedbacks.

The Antarctic sea ice cover is highly seasonal and, unlike the Arctic, there is very little multiyear sea ice (Maksym et al. 2012). Sea ice forms from frazil crystals that float to the ocean surface and accumulate, eventually forming a sheet of ice that thickens and expands over the winter. Thermodynamic sea ice thickening

Denotes content that is immediately available upon publication as open access.

Corresponding author: R. C. Frew, r.frew@pgr.reading.ac.uk

DOI: 10.1175/JPO-D-18-0229.1

occurs at the base of the sea ice during winter due to a vertical conductive heat flux up through the sea ice, forming congelation (columnar) ice. Thicker sea ice grows more slowly due to a reduced conductive heat flux, which acts as a negative feedback on ice thickness during the growth period. Sea ice growth results in a flux of brine into the ocean as the salt is rejected from the ice crystals, which promotes enhanced vertical mixing in the ocean. Summer sea ice melt results in a flux of freshwater to the ocean aiding restratification of the water column. During spring and summer the higher albedo of sea ice relative to open ocean means that a reduction in sea ice concentration (SIC) results in more solar shortwave radiation being absorbed, causing the SIC to reduce further. The albedo feedback has been shown to be a significant contributor to Arctic amplification of global warming (Pithan and Mauritsen 2014).

Unlike in the Arctic, in the Southern Ocean there is very little surface melting of the sea ice as it is covered by a thicker layer of snow and surface air temperatures are much colder. The snow acts to insulate the sea ice, slowing the rate of sea ice thickening and reflecting most of the incoming shortwave radiation. The thick snow layer also means that surface melt ponds are uncommon on Antarctic sea ice (Scott and Feltham 2010), whereas in the Arctic they are prevalent and contribute to the albedo feedback. The relatively thin ice and high snowfall rates in the Southern Ocean mean that snow ice formation is widespread (Fichefet and Morales Maqueda 1999; Massom et al. 2001). Snow ice forms if the weight of snow is great enough to force the snow–sea ice interface below the surface of the seawater, flooding the submerged snow with seawater that then freezes. The net Southern Ocean sea ice response to a snowfall increase is likely to be more sea ice (Powell et al. 2005), however the response is thought to be regionally variable, as shown in a modeling study by Wu et al. (1999), depending on whether there is sufficient snow for snow flooding to occur. It is currently unclear what role snow related processes may have played in the observed Antarctic sea ice changes, as there are large disagreements in the snowfall trends between different reanalysis products (Bromwich et al. 2011).

Sea ice is continuously moved around, primarily by the winds and also by the ocean currents. This can cause the sea ice to break up, potentially piling up and thickening in particular regions, for example, to the east of the Antarctic Peninsula. Trends in the wind fields are able to explain some of the observed trends in sea ice concentration (Holland and Kwok 2012).

Increased ocean stratification has been suggested to play a role in the observed long-term increasing Antarctic sea ice trend (Parkinson and Cavalieri 2012) through a reduction in basal melting, with a number of possible triggers:

(i) Increased snowfall*:* An accelerated hydrological cycle (resulting in more snowfall in the Southern Ocean; Liu and Curry 2010) may lead to a freshening of the surface ocean, increasing stratification. The cooler, fresher surface ocean then promotes increased sea ice growth, due to the reduced ocean–ice heat fluxes and increased freezing point.

(ii) Sea ice–ocean coupled response to atmospheric perturbations*:* On seasonal time scales the change in stratification may be created or amplified by changes to the sea ice–ocean freshwater fluxes in response to increased atmospheric temperatures (Bitz et al. 2006; Zhang 2007; Kirkman and Bitz 2011). An increase in Antarctic sea ice can occur in response to atmospheric warming due to the negative feedback loop between the ice growth rate, and entrainment of warm deep waters. For this scenario to occur, the reduction in basal ocean melting of sea ice is larger than the decrease in ice growth due to atmospheric warming (Martinson 1990; Zhang 2007). However, on interannual and longer time scales the feedback loop associated with changes in ice growth is positive (Goosse and Zunz 2014). Increased sea ice in a region increases the stratification (reducing entrainment of warm deep waters) due to the inflow of freshwater to the region (sea ice melt) and transport of brine (sea ice growth) to deeper in the water column (Goosse and Zunz 2014; Lecomte et al. 2017).

(iii) Ice sheet melt*:* Increased freshwater flux to the surface ocean due to accelerating ice sheet melting (Bintanja et al. 2013; Haid et al. 2017), although the sea ice sensitivity to freshwater injection experiments is inconsistent between models (Swart and Fyfe 2013; Pauling et al. 2016).

(iv) Wind driven freshwater fluxes*:* A change in Ekman pumping caused by a change in the surface wind field.

The interactions between processes i–iv above and atmosphere feedbacks and interactions with the ice cover and ocean likely play a role in the observed changes in Antarctic sea ice. We do not seek to address these broad issues but instead seek clarity on the nature of the response of the sea ice–ocean system to change in the atmospheric forcing, including snowfall, and sea ice–ocean thermohaline interactions (addressing processes i and ii above). We note that Antarctic sea ice plays a crucial role in transforming water masses within both branches of the Southern Ocean limb of the overturning circulation (Abernathey et al. 2016) and

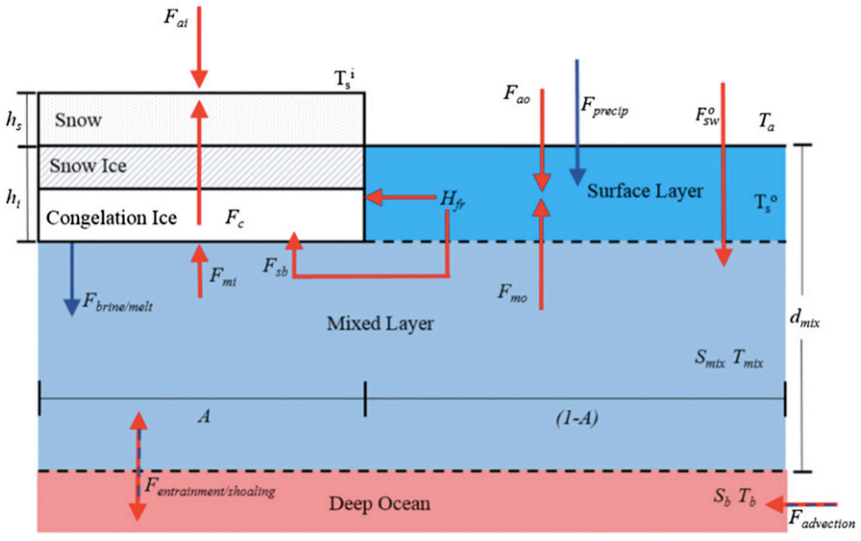

FIG. 1. Schematic of the sea ice–mixed layer model. Heat fluxes are in red, and freshwater/salt fluxes are in navy blue. Adapted from Petty et al. (2013).

understanding trends in this transformation process (Haumann et al. 2016).

Sea ice and ocean interactions and feedbacks around Antarctica are subtle, complex and difficult to elucidate either from observations or coupled climate models. There is a need for a conceptual model/understanding of the important feedbacks and processes in the Southern Ocean sea ice–atmosphere–ocean system, to better understand Antarctic sea ice variability in both warm and cold Antarctic shelf ocean regimes. We have developed and utilized a new version of the zero-dimensional sea ice–mixed layer model described in Petty et al. (2013), with the main addition being a prognostic snow layer and the inclusion of snow-ice formation. The advantage of a simple coupled sea ice–mixed layer model is that it allows interpretation of causality, and through manipulation of boundary conditions, isolation of different processes and analysis of feedbacks. We focus our study on the Amundsen and Weddell Seas. The Amundsen has warm continental shelf waters, and much warmer and wetter atmospheric conditions. In contrast the Weddell has much colder, saltier shelf water properties created by deep ocean mixing driven by cold, dry atmospheric conditions (Petty et al. 2013). The contrasting atmospheric and oceanic conditions in the two regions allows a comparison of the processes and feedbacks that govern sea ice and mixed layer changes in two different regimes.

Our paper is structured as follows. The sea ice–ocean mixed layer model with its new snow-ice parameterization scheme is presented in section 2, with additional model equations presented in appendix A; the ocean and atmospheric forcing fields used are presented in section 3; and reference state results for the two regions are presented in section 4. This is followed by an investigation into the sensitivity of the sea ice and mixed layer to perturbations in the atmospheric forcing fields in section 5. The response of five different feedbacks to surface air temperature perturbations are investigated: ocean feedback, sea ice feedback, the albedo feedback, the insulation feedback, and the freezing temperature feedback. These results are presented and discussed in section 6, followed by a summary and concluding remarks in section 7.

2. Sea ice–ocean mixed layer model

Our sea ice–mixed layer model is based on the zero-dimensional coupled sea ice mixed layer model used in Petty et al. (2013). The coupled mixed layer–sea ice model (see the schematic in Fig. 1) uses the balance of heat fluxes at the sea ice–air and ocean–air interfaces to calculate the surface temperatures. Energy balance equations are used to calculate basal and lateral freezing/melting of sea ice. The entrainment rate is calculated from a balance of buoyancy fluxes and turbulent mixing (from wind shearing) and the mixed layer temperature and salinity are calculated from balance equations. The ambient water properties (temperature and salinity) below the mixed layer are given by vertical profiles that relax back to the imposed, initial profile after shoaling of the mixed layer. The governing equations are outlined in Petty et al. (2013) and are reproduced in appendix A, and the constants and fixed parameters used are in

appendix B. Modifications to the model presented in Petty et al. (2013) are the inclusion of snow ice formation and a prognostic snow layer, described next.

Snow and snow ice

In the original (Petty et al. 2013) model, the snow layer had a fixed depth. This has been adapted so that the thickness of snow h_s is governed by

$$\frac{dh_s}{dt} = P - S - F, \tag{1}$$

where P is the rate of precipitation (assumed to be all snowfall), S is the rate of sublimation, and F is the rate of snow ice formation. There is assumed to be no surface melting of the snow.

If the ice expands laterally, the existing snow layer is redistributed to conserve the mass of snow. This decreases the average snow thickness, reflecting the increase in newly formed sea ice which is not yet snow covered. If the ice concentration decreases, then the snow covering that area of ice also melts and acts to freshen the mixed layer, in this instance the snow thickness remains the same, but the volume has decreased. Under all scenarios the albedo of the (snow covered) ice fraction remains constant.

Whenever the weight of snow is great enough it pushes the snow–ice interface below the surface of the ocean so that the snow that is below the ocean surface floods with seawater and freezes to form snow ice. Sampled snow ice is found to be saltier than congelation sea ice, which we have assumed to be 5 psu. We set the salinity of the snow ice formed to be 10 psu in the model, which falls within the observed range of values (Jutras et al. 2016). This means that the volume of brine release per unit volume of snow ice formed is lower than that of congelation ice formation. In the situation that all the congelation sea ice below has melted, and the snow ice is melting, less freshwater per unit volume will be released into the mixed layer.

Assuming that the snow and sea ice are in hydrostatic balance, with the ice/snow interface at sea level,

$$\rho_i h_i + \rho_s h_s = \rho_{\mathrm{sw}} h_i, \tag{2}$$

where ρ_i is the density of sea ice (both congelation and snow ice), ρ_{sw} is the density of seawater, ρ_s is the density of snow, h_s is the thickness of snow, and h_i is the total sea ice thickness (congelation + snow ice). The relatively small variations in density between congelation and snow ice is assumed to be small enough to be neglected in this simple model.

On a given time step of Eq. (1) the snow ice interface lies below sea level whenever

$$h^* = h_s - \frac{(\rho_{\mathrm{sw}} - \rho_i)h_i}{\rho s} > 0. \tag{3}$$

In this case we instantly create snow ice so that $h_i \rightarrow h_i + \delta h$ and $h_s \rightarrow h_s - \delta h$, where δh is the thickness of submerged snow. Due to the influx of seawater flooding the submerged snow the mass of snow ice formed is not equal to the mass of snow lost; we set the thickness of snow ice formed equal to the thickness of snow lost.

Choosing δh such that Eq. (2) is satisfied yields

$$\delta h = \frac{\rho_s}{\rho_s + \rho_{\mathrm{sw}} - \rho_i} h^*. \tag{4}$$

The effective salinity (after partial brine escape) of the water that is trapped in the submerged snow S_{trap} is given by

$$S_{\mathrm{trap}} = \frac{S_{\mathrm{si}}}{1 - \dfrac{\rho_s}{\rho_i}}, \tag{5}$$

where $1 - (\rho_s/\rho_i)$ is the snow pore fraction. The salt flux into the mixed layer due to snow ice formation, F_{si} for a given sea ice concentration A is then given by

$$F_{\mathrm{si}} = \begin{cases} (S_{\mathrm{mix}} - S_{\mathrm{trap}})\left(1 - \dfrac{\rho_s}{\rho_i}\right)\dfrac{dh}{dt}A, & \text{for} \quad \delta h > 0 \\ 0, & \text{otherwise}, \end{cases} \tag{6}$$

where S_{mix} is the mixed layer salinity, S_{si} is the salinity of the snow ice formed, and dh/dt is the rate of snow ice thickening. The associated heat release from snow ice formation is assumed to be predominantly lost to the atmosphere and is neglected in the model.

3. Boundary forcing and initial conditions

The sea ice–ocean model is driven by atmospheric boundary forcing and integrated forward in time from initial ocean and ice conditions using a finite differences scheme written in FORTRAN.

a. Ocean and sea ice

Our model is initialized with representative summertime profiles of temperature and salinity for the Amundsen and Weddell Seas that are the same as those used in Petty et al. (2013). The profiles are shown in Fig. 2. Observations of the Amundsen Sea suggest a surface layer of near-freezing water, typically extending to a depth of 200 m (Walker et al. 2008; Jacobs et al. 2011), although observations of the depth of this layer do range from 100 to 300 m (Jacobs et al. 1996; Dutrieux et al. 2014). Below the mixed layer, observations

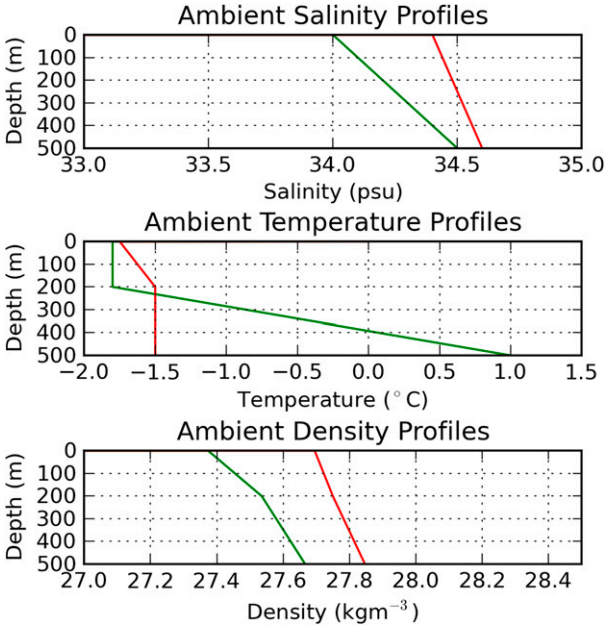

FIG. 2. Ambient ocean profile for the Weddell Sea in red and the Amundsen Sea in green.

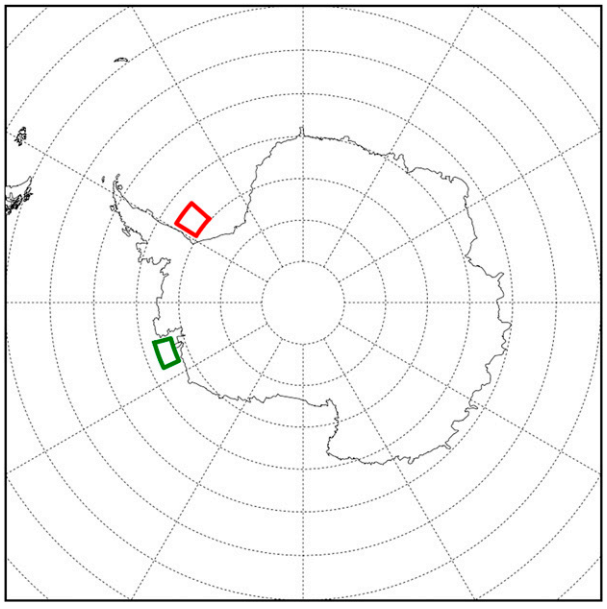

FIG. 3. Latitude–longitude boxes used for spatial averaging of atmospheric forcings. The Weddell Sea is marked in red, and the Amundsen Sea is marked in green.

indicate that the temperature rises up to values of +1°C at about 600 m. The Amundsen shelf sea is filled with warm (+1°C) Circumpolar Deep Water (CDW; Jacobs et al. 1996, 2011; Walker et al. 2008). CDW intrudes beneath the ice shelves in the Amundsen Sea, where, as a result of basal melting, it is implicated in ice loss from West Antarctica (Shepherd et al. 2004). The salinity increases approximately linearly from 33.8 to 34 at the surface to 34.5 at 600 m (Walker et al. 2008; Dutrieux et al. 2014). Our temperature and salinity profiles used for the Amundsen Sea simulations are in good agreement with these observations.

The Weddell Sea has a much less stratified profile, with higher salinity values than in the Amundsen Sea, ranging from values of 34.4 at the surface to approximately 34.6 at 600 m (Nicholls et al. 2003, 2008). High Salinity Shelf Water (HSSW) is formed in the Weddell Sea, which is a precursor to Antarctic Bottom Water. HSSW is predominantly formed in this region from relatively warm Modified Weddell Deep Water (MWDW) that is salinified and cooled due to sea ice growth over the continental shelf (Renfrew et al. 2002; Nicholls et al. 2009). The temperature of the waters from mid depth to the continental shelf is observed to be −1.5°C (Nicholls et al. 2003, 2008). Winter observations of the region are limited due to the treacherous conditions. Winter observations available for the region indicate that winter mixing in the southwestern part of the Weddell Sea continental shelf is deep, with estimates ranging from 100–200 m (Wilson et al. 2019) up to 400 m, and at times spanning the depth of the observed profiles (Nicholls et al. 2008). The Weddell temperature and salinity profiles are designed to reflect the MWDW source waters on to continental shelf, based on observations taken from the southwestern (Nicholls et al. 2003, 2008) and northwestern Weddell Sea (Gordon 1998; Nicholls et al. 2004). Note that denser, more saline HSSW has been found in the south western boundary of the Weddell Sea (Nicholls et al. 2003), with salinities up to 34.8, however this is believed to be formed by the coastal polynya in this region and therefore is not what we seek to represent. After mixed layer shoaling, temperature and salinity are restored to these profiles during the simulations over a time scale of three months, mimicking ocean advection.

b. Atmospheric boundary forcing

ERA-Interim (ERA-I) reanalysis data (Dee et al. 2011) were used to create climatological forcings. The forcing data have been spatially averaged over the boxed regions in Fig. 3 and temporally averaged over 38 years (1979–2016) from 12-h data. The fields are shown in Figs. 4 and 5; the black lines show the smoothed (15 day) climatological forcing fields. The smoothed upper and lower standard deviations ($\pm\sigma$) are plotted in red and blue (for precipitation the 84th and 16th percentiles are used, due to the skewed distribution) and are calculated using a 2.5-day averaging window. The 2.5-day time scale is the auto-decorrelation time scale, taken to be the time for weather systems

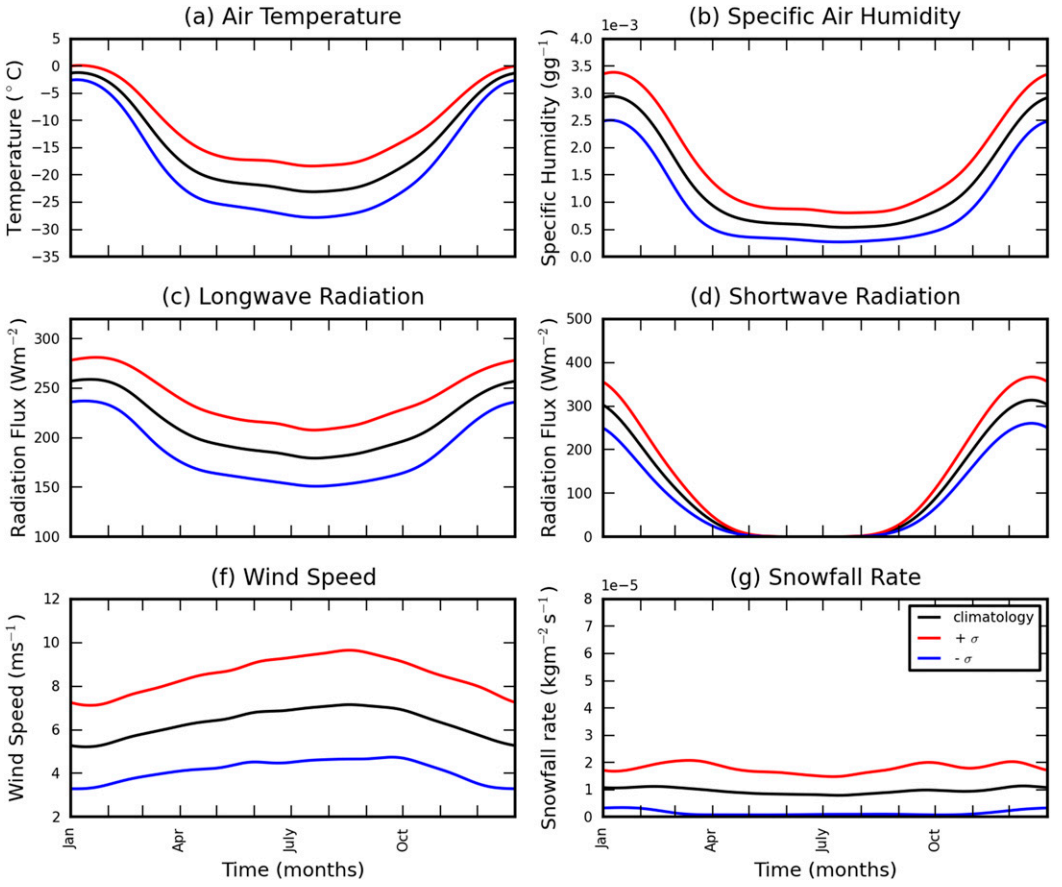

FIG. 4. Climatology for the Weddell Sea, calculated from ERA-I reanalysis, 1979–2016, over the latitude–longitude region 58°–48.5°W, 72°–74.8°S.

to pass over the modeled regions. The 2.5-day averaging window was used to reduce the impact of short-period, high-amplitude variability present in the forcing fields caused by storms, on the standard deviations. The wind speed is cubed in Eq. (A16) (in appendix A), which calculates the momentum transfer to the mixed layer; therefore, the wind speed was cubed before any spatial and temporal averaging.

The 2-m surface air temperatures (SATs) show a clear seasonal cycle in both regions. SATs in the Amundsen Sea reach a minimum of −15°C while those in the Weddell Sea reach a lower winter minimum of −25°C. The standard deviation is largest in the winter with the Amundsen Sea region displaying greater variability. Both regions display low variability in the summer where SATs are consistent around 0°C. The 2-m specific humidity is also greater in the Amundsen than in the Weddell Sea, as would be expected due to the cold, dry katabatic winds coming off from the continent in the Weddell Sea region. In the Amundsen Sea the standard deviation seen is larger in the winter than in the summer, but in the Weddell Sea the standard deviation is more uniform throughout the year, and is just slightly larger in the winter. The incoming longwave radiation also shows slightly greater variability in the winter, with the Amundsen Sea displaying greater variability than the Weddell Sea region. The incoming shortwave radiation shows a clear seasonal cycle which is similar in both regions, going from $0\,\mathrm{W\,m^{-2}}$ in the winter to a maximum of $300\,\mathrm{W\,m^{-2}}$ in the summer, when the maximum standard deviation is shown. The wind speed is greater in the Amundsen Sea by around $1\,\mathrm{m\,s^{-1}}$. Both regions display a similar standard deviation all year round, and a seasonal cycle that has an amplitude of $2\,\mathrm{m\,s^{-1}}$. The snowfall rate and interannual variability is greater for the Amundsen Sea. Typical snowfall values in the Amundsen Sea are $1.5 \times 10^{-4}\,\mathrm{kg\,m^{-2}\,s^{-1}}$ and in the Weddell Sea are $1 \times 10^{-5}\,\mathrm{kg\,m^{-2}\,s^{-1}}$.

4. Reference simulations of sea ice and ocean in the Amundsen and Weddell Seas

Simulations were carried out with the model set up described in section 2 and the climatological atmospheric

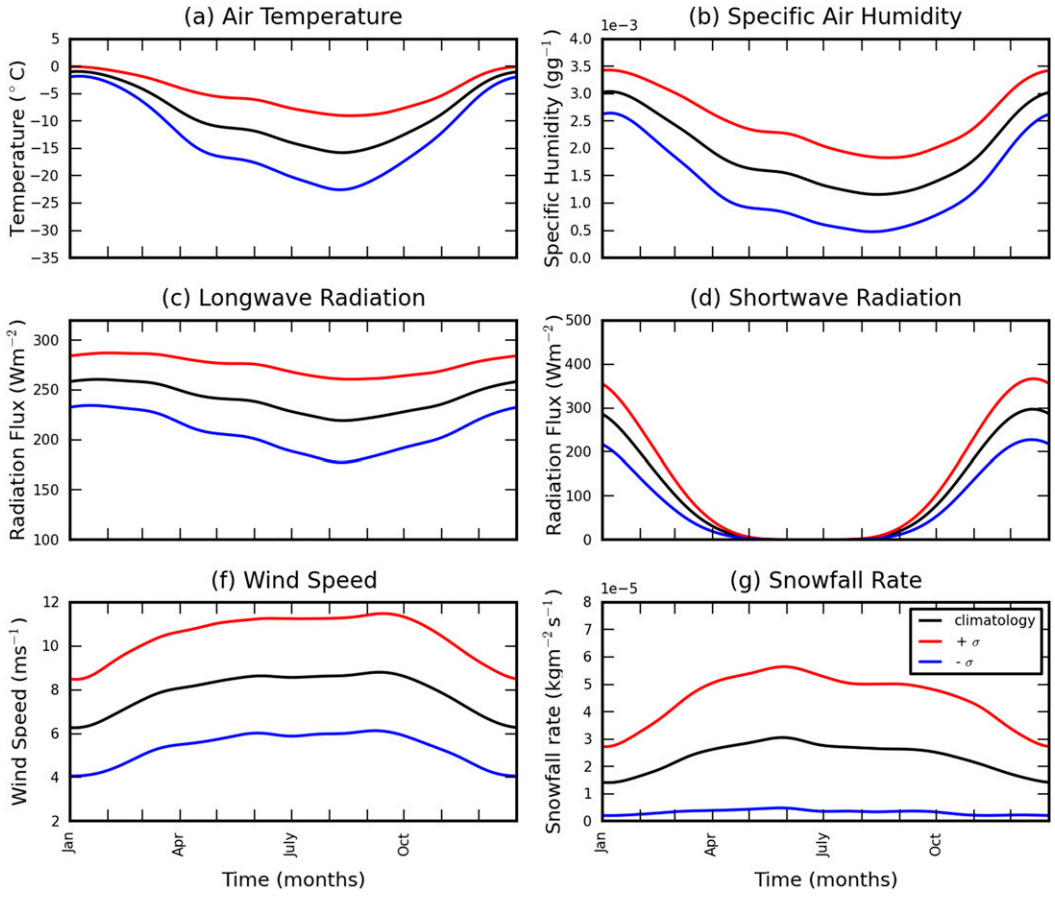

FIG. 5. Climatology for the Amundsen Sea, calculated from ERA-I reanalysis, 1979–2016, over the latitude–longitude region 115°–105°W, 71.5°–73.5°S.

forcing in order to establish a reference state for each region, presented in Figs. 6 and 7.

In the Weddell Sea (Fig. 6) the mixed layer reaches the continental shelf every winter, the ice concentration varies between 0.6 and 1.0 every year, and the ice thickness varies between about 1 and 1.75 m. Snow ice forms between 25% and 60% of the sea ice. The secondary, smaller decrease in ice concentration after the main summer minimum is due to the warming of the ocean as the mixed layer deepens into the warm deep waters. The ice concentration then increases again once the mixed layer hits the maximum mixed layer depth. At this point no more heat is added from the ocean and the ocean cools dramatically. This causes a rapid increase in ice concentration to the maximum ice concentration value. The jagged pattern in the snow thickness reflects these changes in ice concentration, as whenever the ice concentration increases the existing snow layer is redistributed to give a new average snow thickness to prevent artificial creation of snow. Snow thickness is also removed by formation of snow ice. In the Weddell simulation the snow ice is formed as the sea ice thickness starts to decrease, which increases the ratio of snow to ice. Snow ice formation halts once the sea ice thickness increases again, at this point the snow ice thickness decreases slightly due to relaxation of ice thickness and snow ice thickness values, representing the advection of ice (of differing composition) through the region (see appendix A, section c, for details).

In the Amundsen Sea (Fig. 7) the ice concentration varies between 0.5 and 1.0 each year, and the ice thickness between 1.2 and 1.8 m. Due to the high snowfall rate, snow ice forms 90%–100% of the sea ice. At the summer ice minimum all of the sea ice is snow ice, as all of the congelation ice at the base melts, and then the snow ice begins to melt. The mixed layer depth reaches 310 m each winter. As the mixed layer penetrates the 200-m thermocline during winter, the ice concentration starts to decrease due to increased ocean heating from below the ice.

Observations of snow ice are sparse; the limited observations indicate that between 8% and 38% of

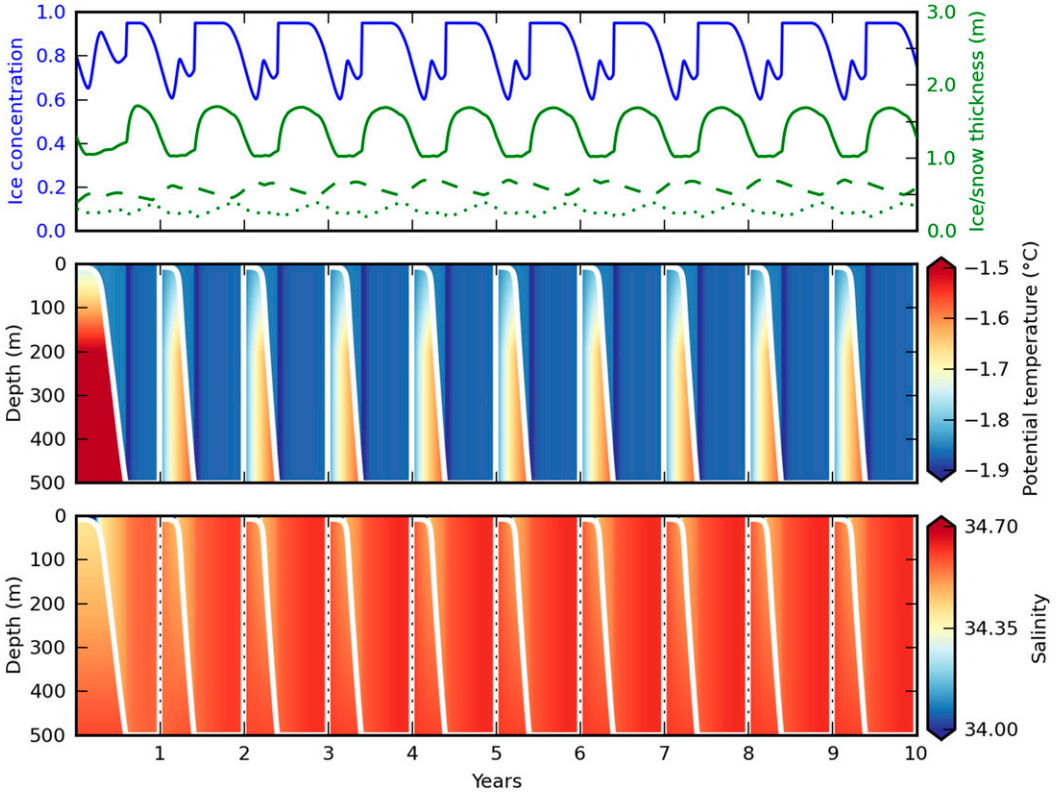

FIG. 6. Results for the Weddell Sea when forcing the model with the climatology. (top) Ice concentration (blue), total (congelation + snow ice) ice thickness (green), snow ice thickness (dashed green), and snow thickness (dotted green), (middle) mixed layer depth (white) plotted over the potential temperature, and (bottom) salinity.

Antarctic sea ice is composed of snow ice (Jeffries et al. 1997; Massom et al. 2001). However, a large range of values have been reported, including much higher values where snow ice makes up nearly all of the sea ice sampled (Massom et al. 2001). In general observations for the Weddell Sea fall at the lower end of estimates (Lange et al. 1990), and those in the Amundsen Sea fall in the upper end of the estimates (Jeffries et al. 1997, 2001). Possible causes of the very high fraction of snow ice in the Amundsen Sea simulations could be a higher snowfall rate in the ERA-I dataset, or a higher basal melt rate than occurs in reality.

5. Sensitivity studies

a. Atmospheric forcing

A set of simulations was performed in which each atmospheric forcing parameter was altered in turn to its $\pm\sigma$ values (plotted in Figs. 4 and 5) with all other forcings given by the climatology. There is large uncertainty in future projections for Southern Ocean climate, however studies suggest that conditions are likely to get warmer and wetter (Christensen et al. 2013), therefore nonlinearity of the response to increasing both surface air temperature and snowfall fields by σ was explored in an additional warmer and wetter (WW) simulation. Note that in this approach we are applying unphysical atmospheric conditions by decoupling atmospheric fields that are not independent.

The sensitivity simulations are summarized in Figs. 8 and 9, where all metrics shown are calculated after 8 years of simulation, to make sure that the model has reached a steady state (this typically only takes 2–3 years).

For the Weddell Sea, the timing of water column destratification and the mean ice volume were chosen as metrics to compare the mixed layer and sea ice sensitivity in Fig. 8. In the Weddell Sea simulations the mixed layer always reaches the continental shelf during winter, meaning that a different metric to the maximum mixed layer depth used in the Amundsen Sea had to be used to summarize mixed layer changes. The timing of mixed layer destratification and the duration spent with the water column completely destratified was found to be important in determining the timing of the sea ice thickness and concentration increase, which coincide with dramatic cooling of the water column as the water column completely destratifies. The winter growth

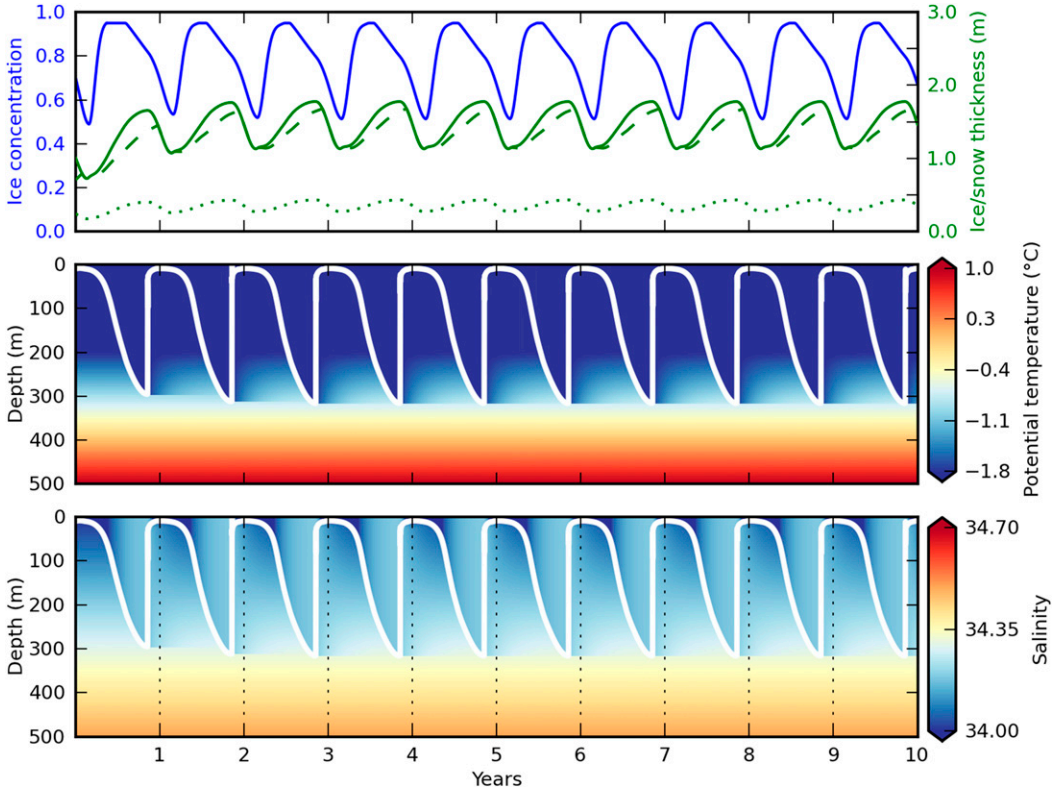

FIG. 7. Results for the Amundsen Sea when forcing the model with the climatology. (top) Ice concentration (blue), total (congelation + snow ice) ice thickness (green), snow ice thickness (dashed green), and snow thickness (dotted green), (middle) mixed layer depth (white) plotted over the potential temperature, and (bottom) salinity.

period generally coincides with the time where the mixed layer is completely destratified. An earlier destratification also means that there is thicker sea ice, as there is a longer period of sea ice growth. For the Amundsen Sea, the maximum mixed layer depth was used in Fig. 9, this was found to be important as it determines how much warm deep water is entrained. Mean ice volume was used to compare sensitivity of the sea ice in both regions.

1) DISCUSSION OF WEDDELL SENSITIVITY RESULTS

Figure 8 shows that greater sensitivity for both the mixed layer and sea ice response was found to shortwave radiation, longwave radiation, and SAT, which all had similar responses of ± 1 month in destratification time, and changes in ice volume of $\pm 0.2\,\mathrm{m}^3\,\mathrm{m}^{-2}$.

The mixed layer and ice volume response to increasing/decreasing each variable by σ is mostly fairly symmetric apart from snowfall. The sea ice and mixed layer responses are generally slightly larger for the $+\sigma$ perturbation to each variable. Most responses are driven by changes in the surface energy balance that promote surface cooling, and therefore ice growth (decrease in SAT, shortwave radiation, longwave radiation, or specific humidity or an increase in wind speed), both these changes drive an earlier water column destratification or vice versa. Increasing wind speed also increases wind stirring, promoting mixed layer deepening. This is only important for shallower mixed layer depths, and the impact of wind speed on the turbulent heat fluxes and the surface energy balance dominates.

Increasing specific humidity reduces the rate of sublimation of snow from the surface, increasing the rate of snow ice formation, slightly increasing the mean ice volume and the rate of destratification. The Weddell Sea ice cover and mixed layer is less sensitive to the perturbations in the snowfall rate than the Amundsen, as the lower snowfall rate means that there is less snow ice formation, and any snow ice that forms generally forms during the spring/summer months when the sea ice is thinner. An increase in snowfall rate increases the thickness of snow ice; this also increases the brine flux into the mixed layer, offsetting some of the impact of the increased surface freshwater flux on the rate of destratification. A decrease in snowfall rate results in less snow ice and faster destratification due to a reduced freshwater flux.

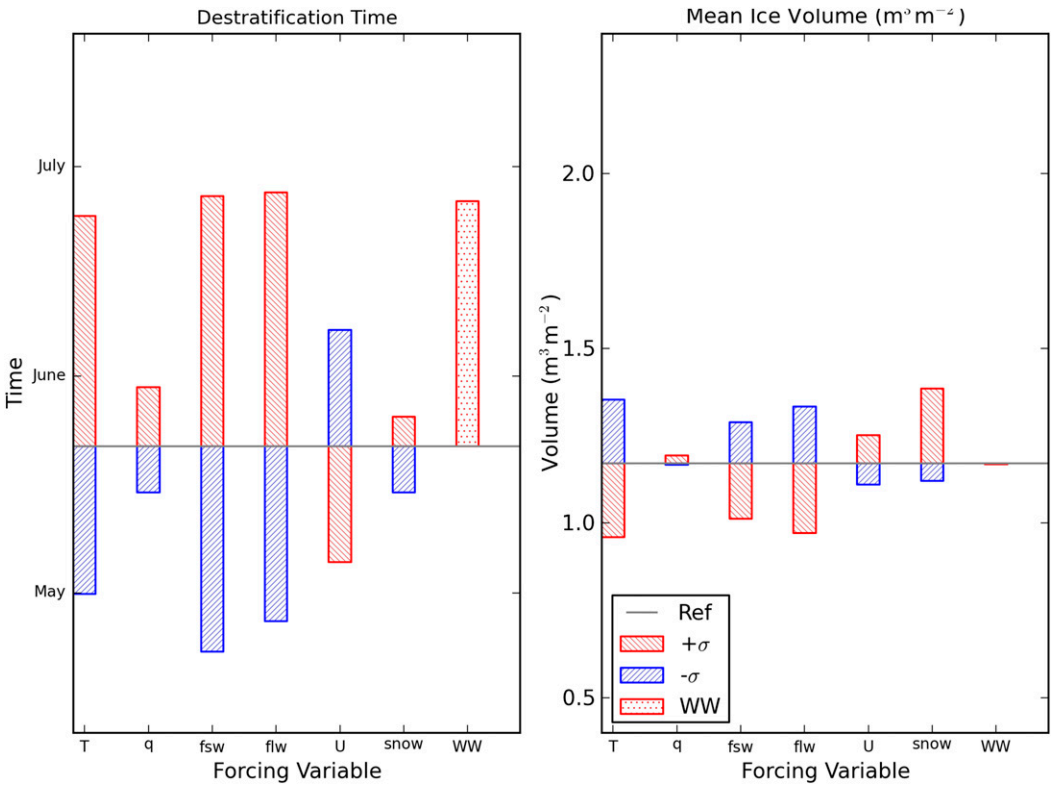

FIG. 8. Sensitivity study results for the Weddell Sea for $\pm\sigma$ of each atmospheric parameter and $+\sigma$ temperature and precipitation (warmer and wetter, WW). The top of each bar is the destratification time/mean ice volume for each perturbed run. The gray line indicates the reference value, and the size and sign of each bar shows the difference between each perturbed run with the reference run value. All values are calculated from when the simulation has reached a steady state.

In the warmer and wetter run ($+\sigma$ SAT and $+\sigma$ snowfall) the impact of increased temperature dominates over the impact of increased snowfall. The sea ice becomes marginally thinner, and the mixed layer destratification slows due to an increased surface freshwater flux from snow and surface warming. Overall, the increase in snow ice and decrease in ice growth due to surface warming balance and result in little change in mean ice volume, although the snow ice fraction of the sea ice increased to become the main component.

2) Discussion of Amundsen sensitivity results

Figure 9 shows that the mixed layer depth displayed the largest sensitivity to the ($-\sigma$) shortwave radiation flux, followed closely by SAT and longwave radiation flux, which all showed changes in the mixed layer depth $\pm$70–80 m. The ice volume showed greatest sensitivity to the snowfall rate, showing a maximum change of just under 1.0 $m^3\,m^{-2}$, followed by specific humidity which resulted in changes on the order of 0.2 $m^3\,m^{-2}$. The Amundsen Sea ice cover showed much less sensitivity to SAT and shortwave and longwave radiation than seen in the Weddell sensitivity results.

Atmospheric perturbations that change the surface energy balance and cause surface cooling promote both increased ice growth and mixed layer deepening. This increases the entrainment of warm deep waters (if the mixed layer is below the 200-m thermocline), acting to decrease the rate of ice growth and therefore ice volume, opposing the direct impact of the atmospheric perturbation on the ice cover. For example, in response to a decrease in SAT, shortwave radiation, or longwave radiation or an increase in wind speed, the ice volume decreases. Changes to the maximum mixed layer depth predominantly impact the summer minimum ice volume, as the maximum mixed layer is reached in early November, around the time that the ice volume is starting to decrease, meaning that an increase in the maximum mixed layer depth will cause the ice growth to plateau and then start to decrease earlier. This negative feedback explains some of the lack of symmetry in the ice volume responses to $\pm\sigma$ perturbations in SAT and shortwave and longwave radiation.

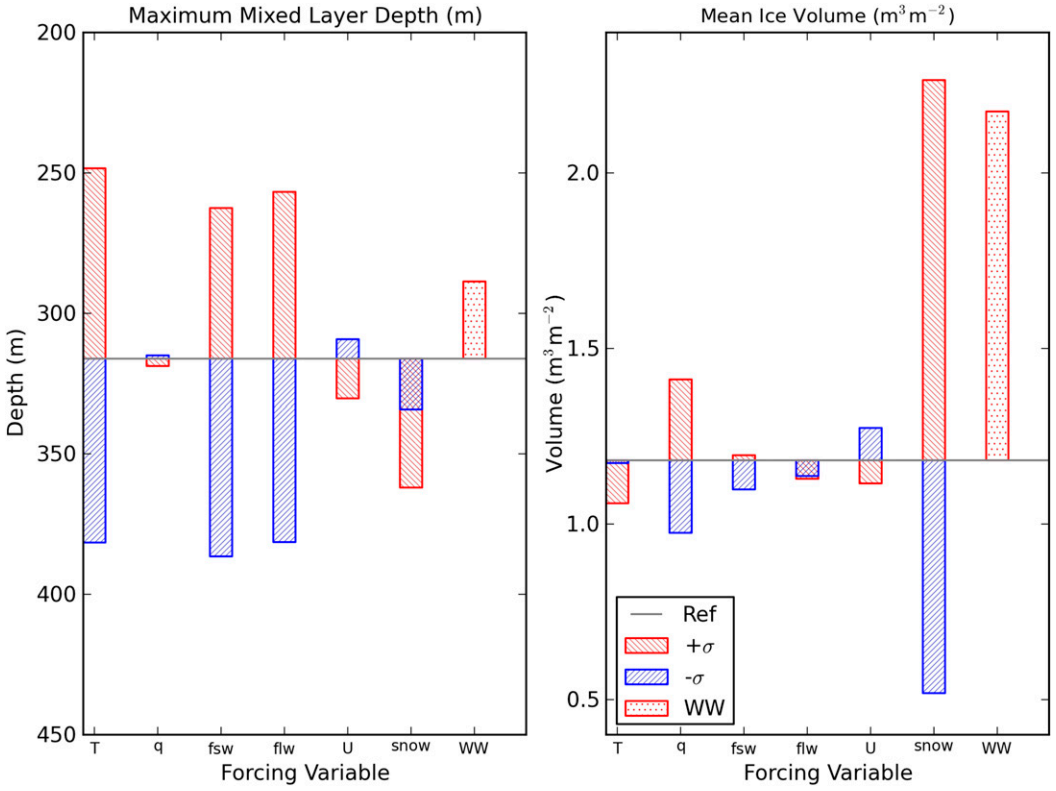

FIG. 9. Sensitivity study results for the Amundsen Sea for $\pm\sigma$ of each atmospheric parameter and $+\sigma$ temperature and precipitation (warmer and wetter, WW). The top of each bar is the maximum mixed layer depth/mean ice volume for each perturbed run. See Fig. 8 for more details.

Similar behavior has been found in other studies (Martinson 1990; Zhang 2007). The relationship between mixed layer deepening and enhanced basal melt means that (i) the ice volume changes in response to perturbations are highly nonlinear, for example, an increase and a decrease in incoming longwave radiation both result in a decrease in the mean ice volume, and (ii) the sea ice volume changes in response to all atmospheric perturbations (except snowfall) are damped and are smaller than those in the Weddell Sea. Both the sea ice volume and mixed layer depth showed a high sensitivity to the snowfall rate, which determines the rate of snow ice formation.

As in the Weddell sensitivity results, decreasing the specific humidity increases the rate of sublimation of snow, decreasing the rate of snow ice formation and decreasing the ice volume. The small change in mixed layer depth reflects both the changes in salt flux from snow ice formation and changes to the surface energy balance (latent heat flux), which in this scenario oppose each other. An increase in the wind speed causes more wind stirring, promoting mixed layer deepening that brings heat into the mixed layer that acts to buffer changes in the ice cover due to changes in the surface energy balance. This causes the resulting changes in mean ice volume for the Amundsen Sea to be the opposite of those in the Weddell Sea in response to changes in wind speed.

The Amundsen Sea ice cover showed greatest sensitivity to the snowfall rate. The relatively thin sea ice and high snowfall rates in the Amundsen Sea region mean that snow ice formation is an important process, forming a majority of the sea ice in the Amundsen Sea simulations. Changes in snowfall also lead to changes in stratification and the amount of basal ocean heating. This means that both increased and decreased snowfall lead to a deeper mixed layer, due to increased snow ice formation (and associated brine flux) or reduced freshwater surface input. However, some caution must be taken in any extrapolation of the Amundsen sensitivity results, particularly to the snowfall rate, as the snow ice fraction in the Amundsen reference simulation exceeds the (limited) range of observations (see section 4).

In the warmer and wetter run ($+\sigma$ SAT and $+\sigma$ snowfall), and in contrast to the Weddell Sea, the impact of the increased precipitation dominates over the increased temperature impact. The sea ice thickens due to the increased rate of snow ice production in response to

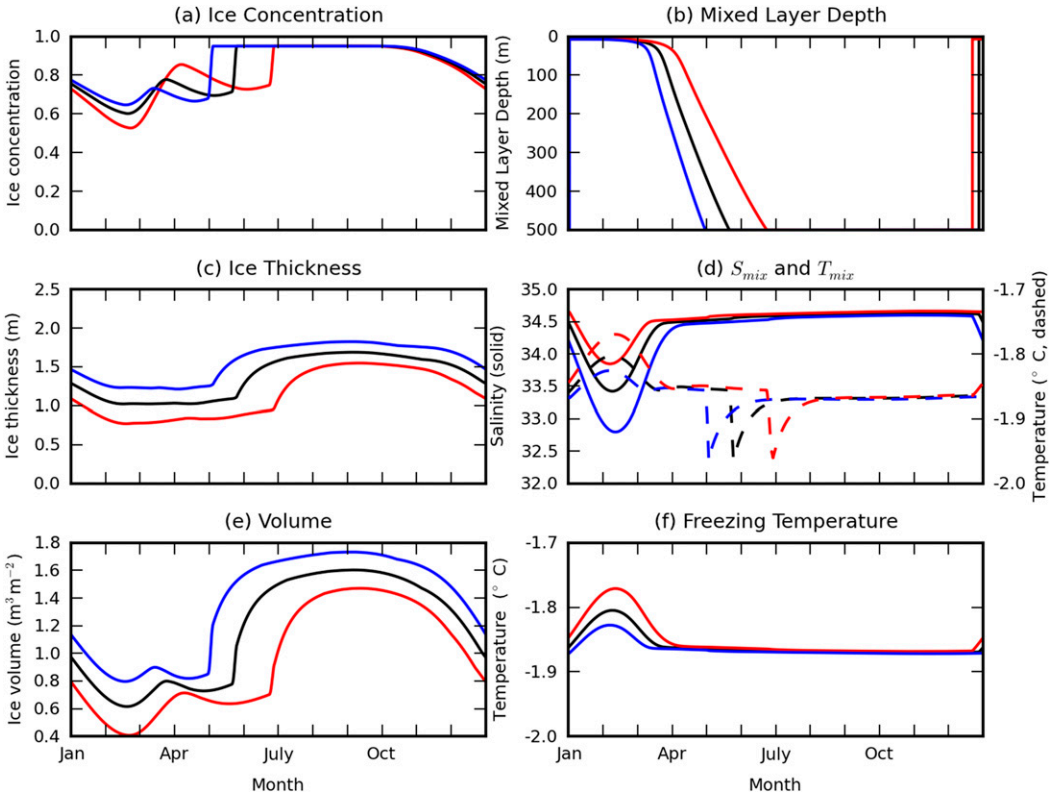

FIG. 10. Steady state ice concentration, mixed layer depth, ice thickness, mixed layer salinity, ice volume, mixed layer temperature (dashed), and freezing temperature (dotted) for the reference (black), $+\sigma$ (red), and $-\sigma$ (blue) SAT runs for the Weddell Sea.

increased snowfall. The mixed layer shoals due to increased freshwater input from snowfall. The shallower mixed layer means that the minimum ice concentration increases due to reduced basal ocean heating.

b. *Discussion of surface air temperature sensitivity studies*

The 2-m SAT perturbations are used in the feedback studies in section 6. SAT was chosen for the feedback studies because both regions demonstrated large sensitivity to it, and it is predicted to increase in the Southern Ocean in CMIP5 models over the next century (Christensen et al. 2013). Although snowfall also fits these two criteria, reanalysis values are not well trusted and predictions have higher uncertainty than surface air temperature (Bromwich et al. 2011; Jones et al. 2016). Plots of the response of the sea ice and mixed layer variables to perturbations in SAT are shown in Fig. 10 (Weddell Sea) and Fig. 11 (Amundsen Sea).

For both regions the $+\sigma$ SATs resulted in thinner sea ice (max and min). In the Weddell Sea the water column destratified later, as shown in Fig. 10, while in the Amundsen Sea the mixed layer was shallower and fresher (deeper and saltier), as shown in Fig. 11. This is predominantly due to a decreased winter conductive heat flux up through the ice, resulting in decreased sea ice growth and therefore decreased brine rejection, which strongly controls the rate of mixed layer deepening, and maximum mixed layer reached. The opposite statements are true for the $-\sigma$ SAT results.

In the Weddell Sea, Fig. 10, the $+\sigma$ SATs resulted in later destratification of the water column, and earlier restratification. The timing of mixed layer destratification determines the timing of ice thickening and expansion as the mixed layer cools dramatically once it reaches the ocean floor as warm deep ocean water is no longer being mixed upward. The whole water column is being cooled, resulting in an increase in ice volume. The rate of winter ice thickening, and the seasonal change in ice thickness is similar in the perturbed and reference runs, the difference being the duration spent near the maximum ice thickness (the winter ice season), which is longer in the cooler case due to the longer duration of the completely destratified water column. For the Weddell Sea the $+\sigma$ SAT run has a larger total change in ice volume, with a later winter increase in ice volume leading to a short winter ice season. The opposite statements are true for the $-\sigma$ SAT run.

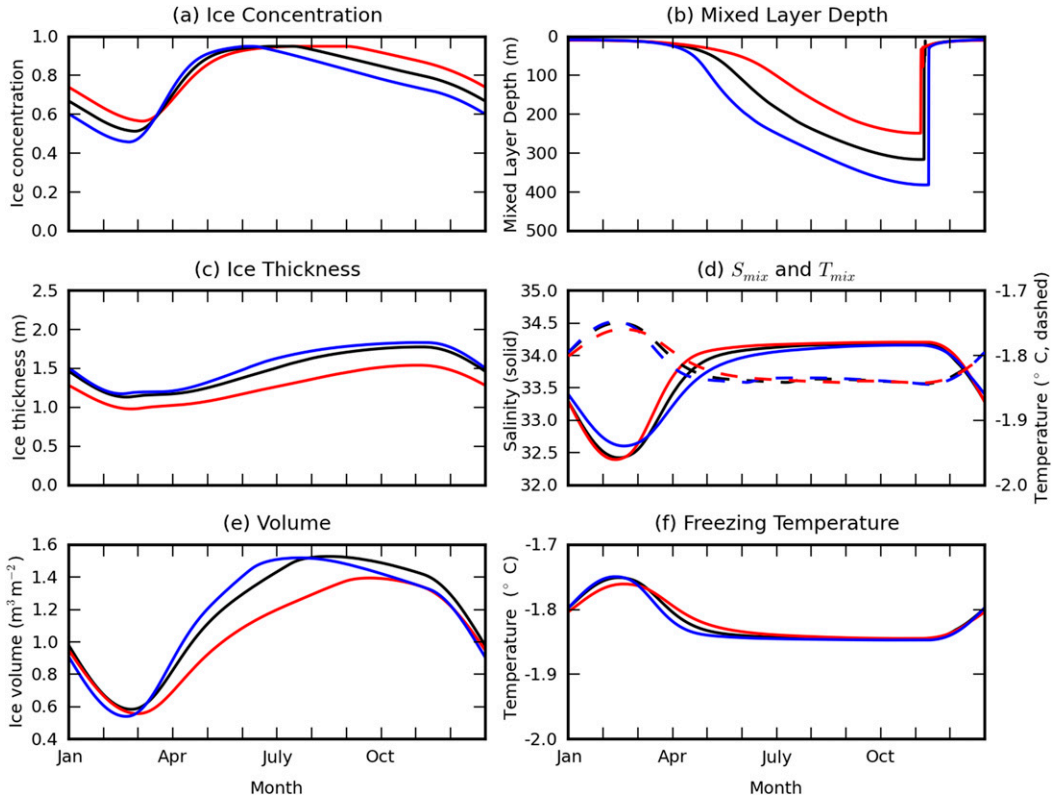

FIG. 11. As in Fig. 10, but for the Amundsen Sea.

In the Amundsen Sea, (Fig. 11) the minimum ice concentration increased slightly in response to $+\sigma$ SATs. Although it appears counter intuitive that warming should increase summer ice concentration and cooling should decrease it, this result is explained by changes in the amount of basal ocean heating, with a decrease in heating associated with a shallower mixed layer. In the $-\sigma$ SAT run the mixed layer is deeper, mixing up more ocean heat, resulting in an earlier spring ice cover reduction (decrease in ice concentration). The opposite scenario is true for the $+\sigma$ SAT run where the mixed layer shoals to above the thermocline. The $-\sigma$ SAT run has the largest seasonal change in volume. Growth is faster than the reference run during the main growth phase and melting starts earlier due to the earlier deepening of the mixed layer below 200 m. In the $+\sigma$ SAT run the seasonal change in ice volume is slightly reduced (the max decreases more than the min), growth is slower, but melting starts later in the year.

In both regions the mixed layer temperature is close to the freezing temperature. In the Amundsen Sea, the mixed layer temperature starts to become very slightly greater than the freezing temperature as the mixed layer deepens into the warmer waters below the thermocline. A similar process happens in the Weddell Sea, except that once the water column becomes completely destratified the mixed layer temperature becomes supercooled, promoting rapid ice growth. In reality this supercooling would result in frazil ice formation, which is not represented in our model.

In both regions there is a reduction in S_{mix} and an increase in T_{mix} during the summer. The salinity decrease is caused by sea ice melting, releasing freshwater into the mixed layer, meanwhile the temperature of the mixed layer increases due to the shallow summer mixed layer and the warmer surface air temperatures. S_{mix} increases as sea ice grows during autumn and rejects brine, and T_{mix} drops. The cooling and salinification of the mixed layer then promotes mixed layer deepening. There is a strong correlation between the dip/hump in the mixed layer salinity and temperature, as they are both dependent on the seasonal change in ice volume. In the Amundsen Sea reference and $-\sigma$ SAT run we can see that the temperature of the mixed layer rises slightly as the mixed layer deepens below 200 m. In the Weddell Sea we see that T_{mix} decreases significantly as the mixed layer completely destratifies the water column. The magnitude of this cooling is not dramatically different, the main difference is the timing of the cooling, which is earlier for the $-\sigma$ SAT run, and later in the $+\sigma$ SAT run.

6. Sea ice–ocean feedbacks

a. Overview

Here we determine the strength and sign of selected feedbacks in moderating the evolution of the sea ice–ocean system in response to perturbations in surface air temperature. In particular we study the impact of feedbacks in the ocean upon the sea ice (ocean feedback denied), feedbacks in sea ice upon the ocean (sea ice feedback denied), the albedo feedback, ice thickness–growth rate (insulation) feedback, and the freezing temperature feedback. Descriptions of the feedbacks along with an outline of how each feedback was denied are in Table 1.

For each feedback we consider the full model with perturbed $\pm\sigma$ SAT and a feedback disabled (FD) run in response to the same $\pm\sigma$ SAT forcing. The difference between the perturbed run and the FD run is the impact of the feedback response to the perturbation in SAT. The metrics are used as for the sensitivity studies, mean ice volume for both regions, timing of water column destratification for the Weddell Sea, and maximum mixed layer depth for the Amundsen Sea. All values are calculated after 8 years of simulation, at which point a steady state has been achieved (this typically only takes 2–3 years). Our feedback results are summarized in Figs. 12 and 13, and described for each region in the following sections. The results are then summarized in section 6c and Fig. 14.

b. Discussion of feedback denial results

1) WEDDELL RESULTS

Feedback denial results for the Weddell Sea are shown in Fig. 12. The distance between the red (blue) cross or dot and the red (blue) line shows the strength of the feedback. When the crosses or dots showing the destratification time/mean ice volume are inside the region bounded by the reference line and the corresponding red/blue line then the feedback is positive, and is negative otherwise.

The ocean FD results show that the ocean processes that are being switched off act as a small negative feedback on the ice volume. In the $+\sigma$ SAT ocean FD run the prescribed water column destratification is earlier, lengthening the winter ice season. However,

TABLE 1. Table outlining the feedbacks studied and how each feedback was denied.

Name of feedback denial simulation	Description of feedback	How the feedback is denied
Ocean denied	Brine rejection from sea ice growth causes mixed layer deepening. This results in more entrainment of warm deep water, increasing basal heating of the ice and reducing ice growth.	Mixed layer depth and properties from the reference run are prescribed.
Ice denied	Sea ice growth and melt results in brine and freshwater input into the mixed layer, resulting in mixed layer entrainment/shoaling. This typically reinforces the impact of atmospheric forcing on the mixed layer, e.g., on seasonal time scales surface cooling promotes mixed layer deepening and sea ice growth, which releases brine into the mixed layer and also causes mixed layer deepening.	The sea ice evolution (ice concentration and thickness) from the reference run is prescribed, along with the corresponding salt and heat fluxes.
Albedo feedback denied	The lower the ice concentration, the more shortwave radiation enters the mixed layer, promoting mixed layer warming and shoaling, causing the ice cover to reduce in concentration.	The ice concentration from the reference simulation is used in Eq. (A11) in appendix A to determine the amount of shortwave radiation entering the mixed layer.
Insulation feedback denied	Thicker (thinner) ice decreases (increases) the conductive heat flux up through the ice (F_c), decreasing (increasing) the rate of ice thickening.	The reference ice thickness has been used within Eqs. (A3) and (A6) in appendix A for F_c and the rate of change of ice concentration (dA/dt).
Freezing temperature feedback denied	Freshening the mixed layer increases the freezing temperature making it harder to melt ice and easier to freeze ice. In the model this relationship is governed by $T_f = 273.15 - 0.054S_{\text{mix}}$. Changes to the S_{mix} in this study are caused by changes to the seasonal cycle in sea ice volume. This is a part of the feedbacks involving changes to the stratification of the Southern Ocean, where freshening and cooling of the surface promote increasing sea ice	The freezing temperature from the reference run is prescribed.

because the mixed layer deepening is earlier, this slows the rate of winter ice volume growth resulting in a decreased mean sea ice volume. Where the mixed layer depth was allowed to evolve in the sensitivity studies, the rate of ice growth determined the time of deepening, meaning that a longer sea ice season corresponded with an increase in mean sea ice volume unlike what is seen when this feedback is removed. The opposite statements are true for the $-\sigma$ SAT ocean FD run. Switching off the ocean response also prescribes the mixed layer salinity and therefore the freezing temperature.

Both ice FD runs have the same destratification time as the reference run. This illustrates that almost all of the mixed layer response to the perturbed surface air temperatures was due to the changes in the seasonal sea ice growth and melt changing the timing and magnitude of brine and freshwater fluxes into the mixed layer.

The albedo feedback acts as weak positive feedback on ice volume, and a slightly stronger positive feedback on the destratification time. In the $+\sigma$ SAT FD run less shortwave radiation entering the mixed layer in the spring results in more summer ice. This increase is not seen as much in the winter ice volume due to negative feedbacks such as the ice thickness–insulation feedback reducing the rate of thickening for thicker ice. The opposite statements are true for the $-\sigma$ SAT FD run.

The insulation feedback acts as a negative feedback on the mean ice volume and the destratification time. In the $-\sigma$ SAT FD run, using the thinner ice thickness increases F_c and results in greater winter ice growth, increasing the mean ice volume and resulting in an earlier destratification time. The opposite is true for the $+\sigma$ SAT FD run.

The freezing feedback only played a significant role in the $-\sigma$ SAT FD run. As shown in Fig. 10, using the higher reference freezing temperature reduces summer ice melt. Denying the freezing feedback increases the mean ice volume by a similar magnitude to the ocean FD, indicating that a significant proportion of the change in ice volume in the ocean FD run may be explained by changes in the freezing temperature. In the $+\sigma$ SAT FD run for the Weddell Sea, however, the mixed layer temperature is roughly equal or greater than both the freezing temperature of the reference run and the warmer case, meaning there is little impact.

2) AMUNDSEN RESULTS

Feedback denial results for the Amundsen Sea are shown in Fig. 13. The results show the ocean FD to strongly buffer the mean ice volume. In $-\sigma$ SAT FD run the prescribed mixed layer is shallower, resulting in an increase in mean sea ice volume. The opposite statements are true in the $+\sigma$ SAT FD run. The large magnitude of response in the ice cover indicates that changes to the depth of the ocean mixed layer strongly buffer the impacts of perturbations in the atmospheric conditions on the sea ice volume. Note that the very small decrease in mean ice volume in the $-\sigma$ run relative to the reference value means that this feedback has a positive sign for the $-\sigma$ SAT FD run.

The ice FD results show that the maximum mixed layer depth are equal to the reference value for both FD simulations. As with the Weddell results, this demonstrates how changes in the sea ice growth, and corresponding brine rejection, are responsible for the mixed layer response to the surface air temperature perturbation. Without the perturbations to the seasonal sea ice evolution the mixed layer remains at the reference value.

The albedo feedback acts as a negative feedback on the maximum mixed layer depth and the mean ice volume. The presence of warm CDW below the 200-m thermocline means that whenever the mixed layer deepens across this depth the amount of heat being mixed upward increases, or decreases if the mixed layer shoals. In the $+\sigma$ SAT FD run the amount of shortwave entering the mixed layer is increased in the spring, shoaling the mixed layer. In the $-\sigma$ SAT FD run, the opposite changes to the shortwave occur. The changes to the mixed layer counteract the decrease in heat transferred to the ice from shortwave fluxes, meaning there is little change in the summer ice volume and a decrease in the winter ice volume is seen. In summary, the presence of the ocean mixing feedback makes the albedo results in the Amundsen Sea nonintuitive for two reasons: (i) the perturbations to the spring and summer ice concentration, which are being used to remove the feedback, are heavily determined by the ocean mixing feedback, and (ii) changes to the shortwave flux into the mixed layer influence the mixed layer depth, therefore making changes to ocean mixing an integral part of the feedback response.

The ice insulation feedback and the freezing temperature feedback show very little impact on the mixed layer depth or mean ice volume. The variation in freezing temperature between the reference and the $\pm\sigma$ SAT runs is not as great as in the Weddell run, as shown in Figs. 10 and 11 due to the ocean mixing feedback buffering changes to the ice volume. This means removing the freezing temperature feedback has little impact, and the changes in the ice volume when removing the ocean mixing feedback are nearly exclusively due to changes in ocean heat. However, larger freshening, for example, from ice sheet melt or continental run off, may make this feedback more important near the continent.

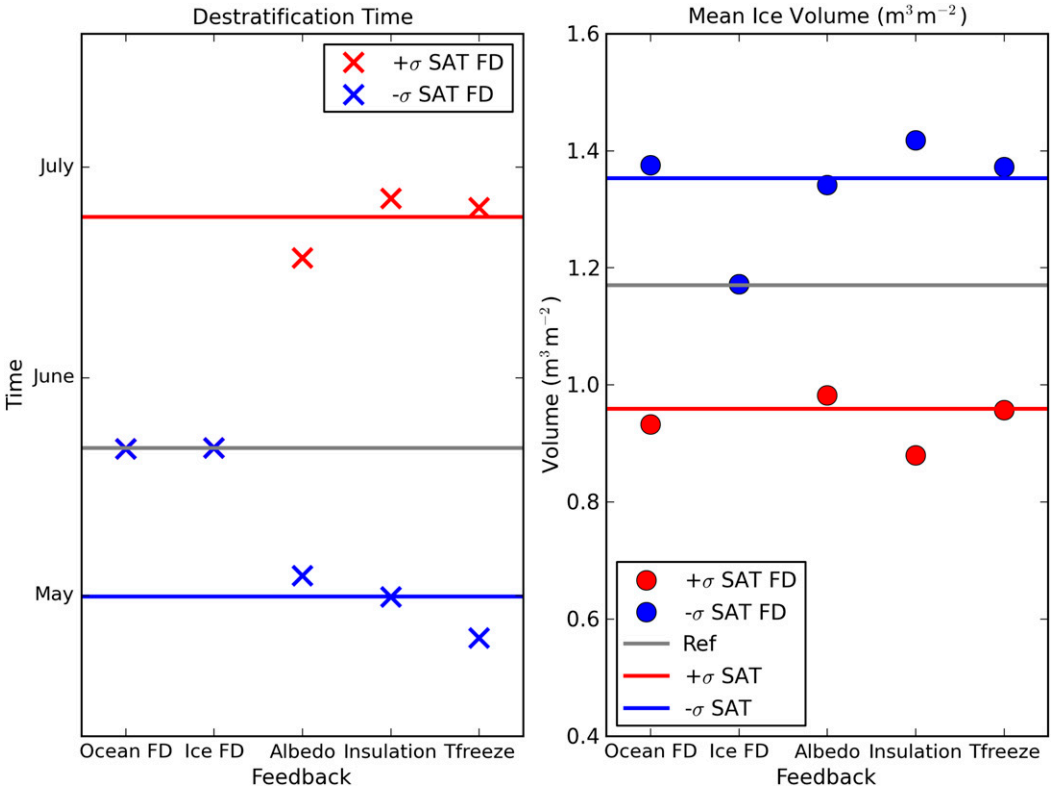

FIG. 12. Feedback study results for the Weddell Sea showing the destratification time and mean ice volume value for each simulation. All values are calculated from when the simulation has reached a steady state.

c. *Summary of feedbacks*

Following the methodology in Goosse et al. (2018), the impact of each feedback on mixed layer depth/destratification time and mean ice volume has been quantified for each set of feedback runs using

$$\gamma = \frac{(\text{Pert} - \text{Ref}) - (\text{FD} - \text{Ref})}{(\text{Pert} - \text{Ref})} = \frac{(\text{Pert} - \text{FD})}{(\text{Pert} - \text{Ref})}, \qquad (7)$$

where γ indicates the sign and relative strength of each feedback for each perturbation and region, Ref is the reference run value (mixed layer depth/destratification timing/mean ice volume), Pert is the perturbed ($\pm\sigma$ SAT) run value, and FD is the corresponding $\pm\sigma$ SAT feedback disabled (FD) run value. The γ gives the magnitude of the feedback impact normalized by the response of the perturbation. A negative value of γ indicates a negative feedback, which acts to dampen any change in mixed layer depth/destratification timing/mean ice volume, meaning that removing the feedback results in amplifying the change. A positive value of γ indicates a positive feedback. Here, $\gamma = 0$ indicates no feedback response (i.e., Pert = FD); $\gamma = 1$ indicates a positive feedback, where all of the response to the perturbation is due to the feedback (FD = Ref), and $\gamma = -1$ indicates a negative feedback where Pert − FD = −(Pert − Ref), meaning that enabling the feedback halves the resulting perturbation.

The use of γ allows the relative size of the feedbacks to be compared for the Weddell and Amundsen Seas relatively easily. The value of γ will be dependent on the reference values and perturbation applied, as discussed in Goosse et al. (2018). This is partially explored by investigating the $\pm\sigma$ SAT response for each feedback. The use of a standard set of perturbations allows us to systematically compare the feedbacks. The feedbacks interact, and influence the impact of other feedbacks. This means that the values of γ corresponding to different feedbacks cannot be simply added to determine the combined feedback response. Figure 14 shows the results for both regions; γ_{ML} is calculated using the maximum mixed layer depth in the Amundsen and using the destratification time in the Weddell, and γ_{ice} is calculated using the mean ice volume for both regions.

In the Weddell Sea, Fig. 14 shows that the ice and mixed layer γ values for the feedbacks are mostly quite consistent for the $\pm\sigma$ perturbations. In the Weddell Sea the impact of the ocean mixing feedback on the ice volume is relatively small. The timing of ice growth and the duration of the winter ice season changes

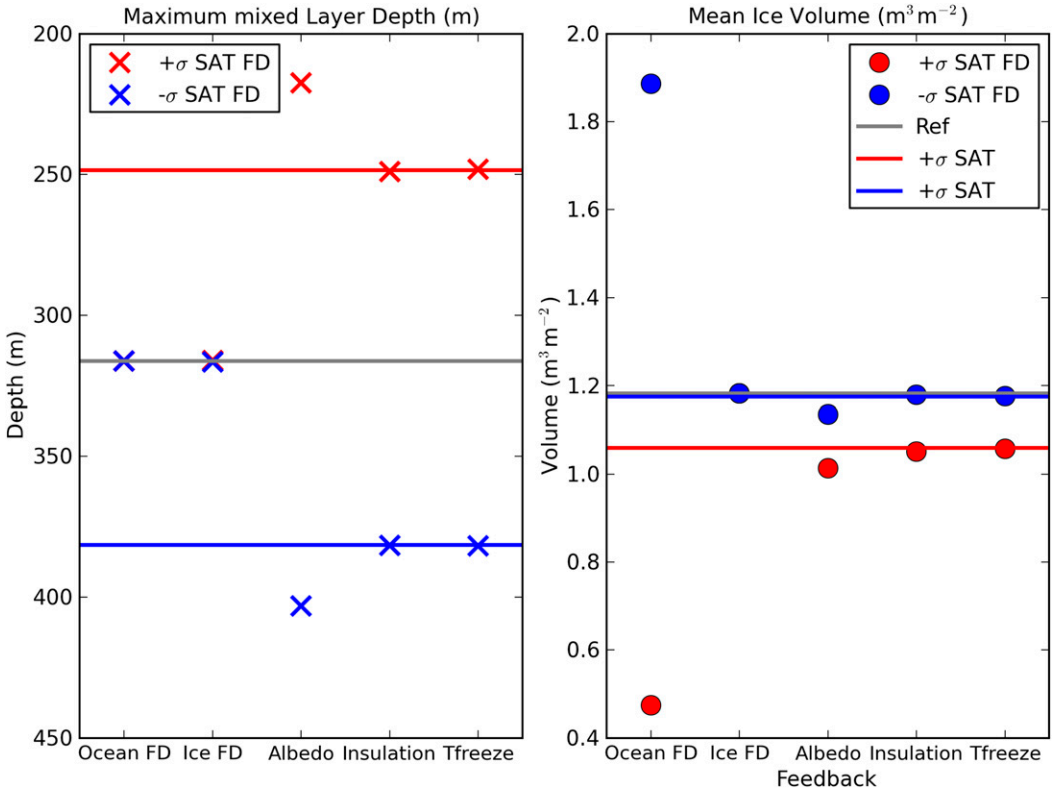

FIG. 13. Feedback study results for the Amundsen Sea showing the maximum mixed layer depth and mean ice volume value for each simulation. All values are calculated from when the simulation has reached a steady state.

(not reflected in γ_{ice}), however there is little change to the ice volume. This is because the mixed layer always destratifies, causing large amounts of water column cooling and ice growth. The ice FD results show that the ice feedback on the mixed layer is strong and positive, reflecting that faster ice growth results in faster destratification. Without the sea ice response to the perturbation the mixed layer remains unchanged, as shown by the γ_{ML} of 1. The albedo feedback in the Weddell Sea is relatively small, but has more intuitive results than the Amundsen (i.e., it is a positive feedback). The insulation feedback has the strongest impact on the ice volume, acting to buffer ice volume changes. The freezing temperature feedback is a weak negative feedback in the $-\sigma$ SAT run, but negligible in the warmer run.

The results in Fig. 14 clearly show how much stronger the impact of the ocean mixing feedback on the ice volume in the Amundsen Sea is than all the other feedbacks studied in both regions. The feedback becomes stronger as the mixed layer entrains deeper into the warm deep waters, making the feedback stronger in the $-\sigma$ FD (off the scale in Fig. 14 with a value of 96.9). This strong feedback means that the changes in ice concentration are relatively small in the sensitivity studies. It also means that the albedo feedback has little impact on the sea ice cover, and actually acts as a negative feedback in the Amundsen Sea. This is because the change in basal heating due to changes in mixed layer depth dominates the ice cover response. As seen in the Weddell the γ_{ML} values for the ice feedback on the mixed layer are 1, illustrating how changes in sea ice growth amplify the impact of the atmospheric perturbation on the mixed layer. Without the changes in sea ice growth the maximum mixed layer depth is unchanged.

The Amundsen Sea mixed layer responses γ_{ML} are fairly consistent in sign for each feedback for $\pm\sigma$ perturbations, however the ice volume responses γ_{ice} are not. The albedo feedback is more negative for the $-\sigma$ run due to the ocean mixing feedback interacting with the albedo feedback, and increasing in strength for deeper mixed layers. The insulation feedback has a very small magnitude in the Amundsen except for the $-\sigma$ mean ice volume which is slightly positive. This is predominantly a result of the very small difference in mean ice volume between the reference and the $-\sigma$ run that is used to calculate γ_{ice}^{lower}. In the Amundsen Sea the freezing temperature feedback has negligible impact on the sea ice cover as differences in the freezing temperature between the $\pm\sigma$ SAT simulations

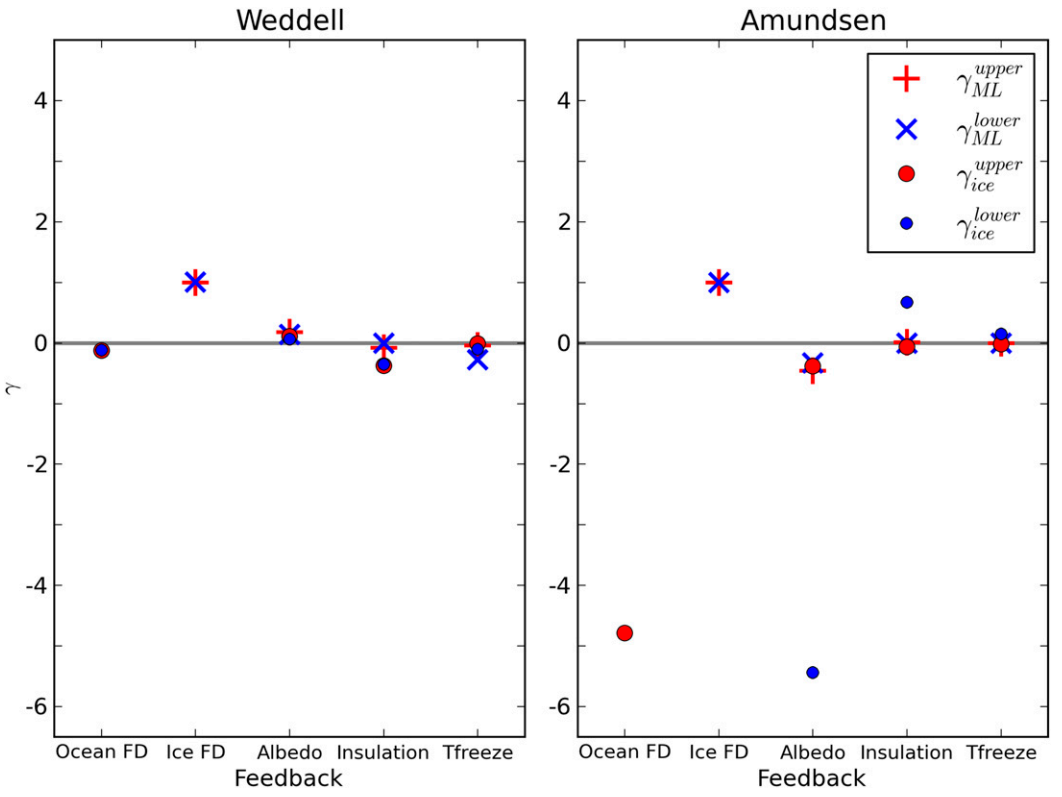

FIG. 14. Values of γ for each set of feedback runs; see Eq. (7) for calculation of γ, indicating the relative magnitude of impact of each feedback on the mixed layer depth/destratification time and mean ice volume for each region. Here γ_{ML} is calculated using the maximum mixed layer depth in the Amundsen Sea and using the destratification time in the Weddell Sea; γ_{ice} is calculated using the mean ice volume for both regions. Note there are no values for γ_{ML} for ocean FD and γ_{ice} for ice FD as the associated mixed layer/ice volume changes are prescribed as part of the process of removing the feedback. The γ_{ice}^{lower} value for the ocean FD in the Amundsen is off the figure scale, with a value of 96.9.

are not large enough to lead to a significant change in ice volume.

7. Summary and concluding remarks

Due to the number and complexity of sea ice interactions the impact of feedbacks on Antarctic sea ice and the ocean mixed layer is currently poorly understood. A new version of the sea ice–mixed layer model described in Petty et al. (2013) has been used to investigate the importance of sea ice–ocean feedbacks in the Amundsen and Weddell Seas, a warm and a cold Antarctic shelf ocean regime. The main additions to the model are a prognostic snow layer and the inclusion of snow-ice formation, which are important for investigating the sea ice sensitivity to the precipitation rate. The model is able to simulate realistic annual sea ice and mixed layer evolution, similar to results in Petty et al. (2013), with the Amundsen Sea partially destratifying (mixed layer depth of 310 m), and the Weddell Sea completely destratifying to the continental shelf (500 m). Using such a simple model allows easier isolation of processes and feedbacks though manipulating the boundary conditions, and allowing subsequent interpretation of the response. Insights from this analysis can be useful for interpreting and addressing inadequacies in more comprehensive models, for example, Petty et al. (2014). However, care must be taken when extrapolating the findings due to the simplicity of the assumptions the model is built on. In particular our model excludes explicit representation of all horizontal transport processes, which are only crudely captured through relaxation of ice and ocean properties to climatological conditions. An analysis of circum-Antarctic sea ice–ocean interactions and feedbacks necessitates a more spatially dependent model.

We explored the sensitivity to each of the six atmospheric forcing variables: SAT, specific humidity, shortwave radiation, longwave radiation, wind speed, and snowfall rate. Each variable was varied individually by $\pm\sigma$, apart from snowfall rate where the 16th and 84th percentiles were used. The response was quantified by the change

in the destratification time of the water column and mean ice volume in the Weddell Sea, and the maximum mixed layer depth and mean ice volume in the Amundsen Sea.

We found a very different sensitivity to surface atmospheric conditions in the two regions. In the Weddell Sea the water column completely destratified during winter in all sensitivity scenarios, however the timing becomes earlier/later depending on whether the rate of sea ice growth is increased/decreased. Decreased winter sea ice growth and a shorter period of complete destratification could decrease the rate of formation of Antarctic Bottom Water, as is currently being observed (Purkey et al. 2019).

In the Amundsen Sea, changes to the surface energy balance that promote ice growth and ocean cooling also promote mixed layer deepening. Changes to entrainment of warm deep waters oppose the direct impact of the atmospheric perturbation on the ice cover through changes in the rate of basal ice melting. These competing processes are evident in the sensitivity responses, and have been found in other modeling studies (Martinson 1990; Zhang 2007). A shallower mixed layer could also result in more warm CDW on the continental shelf, resulting in increased melting of the ice shelves.

Feedback studies were carried out using SAT perturbations and feedback denial experiments. The feedbacks investigated were (i) the ocean feedback, whereby deepening of the mixed layer into warm, deep waters can increase the basal melt rate acting as a negative feedback on sea ice growth; (ii) the sea ice feedback, whereby the seasonal sea ice melt and growth cycle inputs freshwater and brine into the mixed layer, influencing the entrainment rate, typically amplifying the effect of atmospheric perturbations on the mixed layer (e.g., surface atmospheric warming causes both surface ocean warming and an increase in sea ice melt, both promoting mixed layer shoaling); (iii) the albedo feedback, whereby the ice concentration determines how much shortwave radiation enters the mixed layer so that a decrease in ice concentration increases the shortwave radiation flux to the mixed layer, causing shoaling and warming, promoting further decline in the sea ice concentration; (iv) the insulation feedback, whereby thicker sea ice has a lower conductive heat flux up through the ice, reducing the rate of ice thickening, acting as a negative feedback during ice growth; and (v) the freezing temperature feedback, whereby fresher seawater freezes at a higher temperature, meaning that freshening from increased sea ice melt could in turn promote ice growth and act as a negative feedback.

In the Weddell Sea all the feedbacks were found to have a fairly minimal impact on the ice volume when compared to the magnitude of the sensitivity results. The sea ice feedback study showed that sea ice response to the atmospheric perturbation strongly amplified and controlled the mixed layer response. This suggests that while the strong surface cooling is the driver required to destratify the water column, it is the brine rejection from sea ice growth that strongly controls the rate and timing of mixed layer deepening. The same strong relationship was seen in the Amundsen. The albedo feedback is a small positive feedback in the Weddell Sea. The insulation feedback had the strongest impact on the sea ice volume, acting as a negative feedback on ice growth.

In the Amundsen Sea, the results from our feedback studies showed that the mixed layer response to atmospheric forcing acts as a strong buffer against the sea ice response to atmospheric perturbations, increasing/decreasing basal melting due to changes in entrainment of warm deep waters. Quantifying the impact of each of the feedbacks on the mixed layer and ice volume showed that the impact of the ocean feedback on the ice volume was by far the strongest. The impact of the ocean feedback was larger than the ice volume response to the $\pm\sigma$ SAT perturbation, meaning that in the absence of the feedback, the ice response would be several times larger. The negative feedback was shown to strengthen as the mixed layer deepened further into the deep warm waters, opposing changes to the ice cover caused by surface warming. Zhang (2007) also showed that this change in ocean heating may outweigh the change in sea ice growth. This feedback interacts strongly with the other feedbacks investigated, due to the buffering of the ice concentration and ice volume changes in response to the perturbations, influencing the strength and behavior of the other feedbacks. Changes to the mixed layer depth caused by other feedbacks also involve changes in mixing of deep waters, involving the ocean feedback. For example, the albedo feedback involves more or less shortwave radiation entering the mixed layer, which then shoals or deepens the mixed layer, engaging the ocean feedback.

The conditions in the Southern Ocean are predicted to get warmer and wetter (Christensen et al. 2013). The magnitude and regional variation in this is uncertain. The sensitivity results here suggest that reliable precipitation datasets are crucial. An increase in snowfall could promote an increase in the sea ice volume due to two processes: (i) an increase in snow ice formation and (ii) freshening the surface ocean and decreasing the entrainment of warm deep waters. The formation of snow ice releases less brine into the ocean than the same volume of congelation ice from basal freezing, this effectively contributes to surface freshening. Our studies show that the sensitivity to continued warming and increased snowfall in the Weddell Sea response was

dominated by sensitivity to air temperature, resulting in a decrease in sea ice, and slower destratification, whereas the Amundsen Sea response was dominated by sensitivity to increasing snowfall, resulting in more sea ice due to snow ice formation and a shallower mixed layer due to surface ocean warming and freshening.

APPENDIX A

Coupled Sea Ice–Ocean Mixed Layer Model Equations

Our sea ice–mixed layer model is based on the zero-dimensional coupled sea ice–mixed layer model used in Petty et al. (2013). A fuller description of the model can be found in Petty et al. (2013); the basic equations are presented below.

a. Surface heat balance

The snow covered surface ice temperature T_S^i is calculated by balancing the atmospheric surface heat fluxes (sensible, latent, blackbody, incoming longwave, and incoming shortwave heat fluxes) and the conductive heat flux upward through the sea ice as

$$\rho_a c_a C_D^i U_a (T_S^i - T_a) + \rho_a L_s C_D^i U_a [q_{\text{sat}}(T_S^i) - q_a] + \varepsilon_s \sigma (T_S^i)^4 - \varepsilon_s F_{\text{lw}}\downarrow - (1-\alpha_s) F_{\text{sw}}\downarrow = F_c(T_S^i)\uparrow, \tag{A1}$$

and the open water surface temperature T_S^o is calculated by balancing the atmospheric surface heat fluxes with the heat flux from the mixed layer to the open water surface ocean

$$\rho_a c_a C_D^o U_a (T_S^o - T_a) + \rho_a L_s C_D^o U_a [q_{\text{sat}}(T_S^o) - q_a] + \varepsilon_w \sigma (T_S^o)^4 - \varepsilon_w F_{\text{lw}}\downarrow - (1-\alpha_w)[1 - I_o \pm (0)] F_{\text{sw}}\downarrow = F_{\text{mo}}(T_S^o)\uparrow, \tag{A2}$$

where U_a is the wind speed at 10 m, q_{sat} is the saturation specific humidity, q_a is the specific air humidity at 2 m, $F_{\text{lw}}\downarrow$ is the incoming longwave radiation heat flux, $F_{\text{sw}}\downarrow$ is the incoming shortwave radiation heat flux. All other variables and constants are defined in appendix B.

b. Sea ice thermodynamics

The zero-layer sea ice model has been used (Semtner 1976), this assumes that there is a linear temperature gradient through the snow and sea ice, with the conductive heat flux F_c given by

$$F_c = \frac{k_i k_s (T_f - T_S^i)}{(k_i h_s + k_s h_i)}, \tag{A3}$$

where h_i is the ice thickness, h_s is the snow thickness, and T_f is the freezing temperature of seawater (the mixed layer), given as $T_f = 273.15 - 0.054 S_{\text{mix}}$, where S_{mix} is the mixed layer salinity.

The heat flux to the base of the sea ice from the ocean mixed layer F_{mi} is

$$F_{\text{mi}} = \rho_w c_w c_h u_\star^i (T_{\text{mix}} - T_f), \tag{A4}$$

where $u_\star^i$ is the friction velocity between the ice and the mixed layer, and T_{mix} is the temperature of the mixed layer. The heat flux from the mixed layer to the open water surface layer F_{mo} is

$$F_{\text{mo}} = \rho_w c_w u_\star^o (T_{\text{mix}} - T_S^o), \tag{A5}$$

where $u_\star^o$ is the friction velocity between the open water surface layer and the mixed layer.

The rate of change of ice concentration dA/dt is calculated by balancing the ocean surface heat potential, with the latent heat released/absorbed by the ice growth/melt as

$$\frac{dA}{dt} = \begin{cases} \dfrac{H_{\text{fr}}(1-A)}{L_f \rho_i h_i}, & \text{for } A < A_{\max} \text{ and } T_S^o < T_f \text{ (freezing)}, \\ \dfrac{H_{\text{fr}}(1-R_b)(1-A)}{L_f \rho_i h_i}, & \text{for } A > 0 \text{ and } T_S^o > T_f \text{ (melting)}, \\ 0, & \text{otherwise}, \end{cases} \tag{A6}$$

where A is the ice concentration and the ocean surface heat potential H_{fr} is given as

$$H_{\text{fr}} = F_{\text{mo}}(T_S^o) - F_{\text{mo}}(T_f) = \rho_w c_w u_\star^o (T_f - T_S^o), \tag{A7}$$

and $F_{\text{mo}}(T_f)$ is used later in the calculation of the resultant temperature change of the mixed layer, except for when $A = 0$ and $T_S^o > T_f$. Once the ice concentration has expanded to the maximum value so that $A = A_{\max}$, the

ocean surface heat potential is used to grow ice vertically. This vertical growth dh_i^R/dt is considered to be due to redistribution of the sea ice grown in the permanent lead fraction $(1 - A_{\max})$ through pressure ridging.

The parameter R_b is used to partition the melt. $R_b = 0$ when all melt is lateral, and $R_b = 1$ when all melt is basal, giving a basal heat flux $F_{\rm sb}$ of

$$F_{\rm sb} = \begin{cases} -H_{\rm fr} R_b (1 - A), & \text{for} \quad A > 0 \quad \text{and} \quad T_S^o > T_f, \\ 0, & \text{otherwise}. \end{cases} \tag{A8}$$

The rate of basal melting or freezing dh_i/dt depends on the sum of the heat fluxes at the mixed layer–ice interface, which gives

$$\frac{dh_i}{dt} = (F_c - F_{\rm mi} - F_{\rm sb})/(\rho_i L_f), \tag{A9}$$

where a positive (negative) value of dh_i/dt indicates basal ice growth (melting).

c. Ice dynamics

Ice dynamics are predominantly neglected within the model. In Petty et al. (2013) there is a sink of ice concentration due to ice divergence. This has been modified to reflect the influence of ice advection across ice thickness gradients on the vertical structure of the ice. Ice advection is parameterized in the model as a relaxation over time scale τ^*, toward a reference ice concentration $A^{\rm ref}$ and vertical ice structure (total ice thickness $h_i^{\rm ref}$, snow ice thickness $h_{\rm si}^{\rm ref}$, and snow thickness $h_s^{\rm ref}$) values. These reference values represent typical ice concentration and ice thickness values being advected into the simulated region, and are given in Table A1. Physically, this is representing sea ice being flushed through the region, altering the ice concentration, ice thickness, and snow ice thickness.

d. Mixed layer model

1) Surface buoyancy fluxes

The rate of mechanical energy input from surface buoyancy forces to the mixed layer (power input per unit mass per unit area) is computed as

$$P_B = c_2 d_{\rm mix} \left(\frac{g\alpha}{\rho_w c_w} \right) F_T\uparrow - g\beta F_S\uparrow, \tag{A10}$$

where $d_{\rm mix}$ is the mixed layer depth and c_2 is a coefficient characterizing the power dissipation as a result of convective mixing and has a value of 1 (0.8) when the mixed layer is losing (gaining) energy. The heat F_T and salt F_S fluxes out of the mixed layer are given as

TABLE A1. Reference ice and snow values used in advection parameterization for the Amundsen and Weddell model setups.

	Amundsen	Weddell
τ^* (yr^{-1})	0.6	1.0
$A^{\rm ref}$	0.2	0.2
$h_i^{\rm ref}$ (m)	0.5	1.0
$h_{\rm si}^{\rm ref}$ (m)	0.1	0.2
$h_s^{\rm ref}$ (m)	0.2	0.3

$$F_T\uparrow = (1 - A)(F_{\rm mo} - F_{\rm sw}^o\downarrow) + AF_{\rm mi}, \tag{A11}$$

$$F_S\uparrow = \frac{\rho_i}{\rho_\omega}(S_i - S_{\rm mix})\left(\frac{dh_i}{dt}A + \frac{dA}{dt}h_i\right) + (P - E)S_{\rm mix}(1 - A) + F_{\rm sm}\uparrow - F_{\rm si}\uparrow, \tag{A12}$$

where $F_{\rm sm}\uparrow$ is the freshwater flux into the mixed layer from snow whenever the ice concentration decreases, and snowmelt is released into the mixed layer, calculated as

$$F_{\rm sm}\uparrow = \begin{cases} \dfrac{dA}{dt} h_s S_{\rm mix} \dfrac{\rho_s}{\rho_w}, & \text{for} \quad \dfrac{dA}{dt} < 0, \\ 0, & \text{otherwise}, \end{cases} \tag{A13}$$

and $F_{\rm si}\uparrow$ is the salt release into the mixed layer due to snow ice formation, calculated as

$$F_{\rm si}\uparrow = \begin{cases} (S_{\rm mix} - S_{\rm trap})\left(1 - \dfrac{\rho_s}{\rho_i}\right)\delta h_{\rm si} A, & \text{for} \quad \dfrac{dh_{\rm si}}{dt} > 0, \\ 0, & \text{otherwise}, \end{cases} \tag{A14}$$

where $S_{\rm mix}$ is the mixed layer salinity (the practical salinity scale is used), P is the precipitation rate, E is the evaporation rate, calculated from the latent heat flux over the open water surface. Note that Eq. (A12) differs from Eq. (13) in Petty et al. (2013). The term representing brine rejection into the mixed layer from ridging has been removed. The thickening here is dynamic, not thermodynamic growth, and therefore should not result in brine rejection. The shortwave radiation that enters the open water fraction is absorbed in the mixed layer (the surface layer is assumed to completely absorb incoming longwave radiation), and is calculated as

$$F_{\rm sw}^o\downarrow = F_{\rm sw}\downarrow(1 - e^{\kappa_w d_{\rm mix}})(1 - \alpha_w)I_0(0). \tag{A15}$$

Over the ice fraction, the snow layer absorbs all nonreflected solar radiation.

2) WIND MIXING

The rate of turbulent kinetic energy (TKE) input from wind stirring into the mixed layer is given by

$$P_w = c_1 e^{-d_{\text{mix}}/d_w} u_\star^3, \tag{A16}$$

where the effective friction velocity at the upper surface of the mixed layer $u_\star$ is calculated, assuming free drift, as

$$u_\star = U_a \sqrt{(\rho_a/\rho_w)[AC_D^i + (1-A)C_D^o]}. \tag{A17}$$

3) MIXED LAYER ENTRAINMENT

The power needed to entrain deep water into the mixed layer at rate w is calculated as

$$P_E = w(d_{\text{mix}}\Delta b + c_m^2), \tag{A18}$$

where c_m is a bulk turbulent velocity scale describing the turbulent fluctuations of the mixed layer that lead to a frictional sink of TKE, and Δb is the buoyancy difference across the mixed layer base

$$\Delta b = g\alpha(T_{\text{mix}} - T_b) - g\beta(S_{\text{mix}} - S_b), \tag{A19}$$

where T_b and S_b are the temperature and salinity directly beneath the base of the mixed layer.

Constructing an energy balance for the mixed layer from Eqs. (A10), (A16), and (A18) gives an entrainment rate

$$w = \frac{dd_{\text{mix}}}{dt} = \frac{1}{d_{\text{mix}}\Delta b + c_m^2}(P_w + P_B). \tag{A20}$$

This equation is used to deepen and shoal the depth of the mixed layer.

The temperature and salinity evolution of the mixed layer are given by the conservation equations for heat and salt

$$\frac{dT_{\text{mix}}}{dt} = \begin{cases} \dfrac{-F_T\uparrow}{\rho_w c_w d_{\text{mix}}} + \dfrac{w}{d_{\text{mix}}}(T_b - T_{\text{mix}}), & \text{for} \quad w > 0, \\ \dfrac{-F_T\uparrow}{\rho_w c_w d_{\text{mix}}}, & \text{for} \quad w \le 0, \end{cases} \tag{A21}$$

$$\frac{dS_{\text{mix}}}{dt} = \begin{cases} \dfrac{-F_S\uparrow}{d_{\text{mix}}} + \dfrac{w}{d_{\text{mix}}}(S_b - S_{\text{mix}}), & \text{for} \quad w > 0, \\ \dfrac{-F_S\uparrow}{d_{\text{mix}}}, & \text{for} \quad w \le 0, \end{cases} \tag{A22}$$

which show that whenever the mixed layer shoals, T_{mix} and S_{mix} can only change through the surface fluxes and not from advection of the ambient properties. This is also true whenever the water column is completely destratified, representing when the mixed layer has reached the shelf seabed.

TABLE B1. Table of variables.

A	Ice concentration
d_{mix}	Mixed layer depth
E	Evaporation rate
F_c	Conductive heat flux through the ice and snow
$F_{\text{lw}}\downarrow$	Incoming longwave radiative heat flux
F_{mo}	Heat flux from the mixed layer to the open water surface layer
F_{mi}	Heat flux into the base of the sea ice at the mixed layer–sea ice boundary
F_{sb}	Basal heat flux
$F_{\text{si}}\uparrow$	Salt flux from snow ice formation
$F_{\text{sm}}\uparrow$	Freshwater flux from snowmelt
$F_{\text{sw}}\downarrow$	Incoming shortwave radiative heat flux
$F_T\uparrow$	Surface heat flux out of the mixed layer
$F_S\uparrow$	Surface salt flux out of the mixed layer
H_{fr}	Ocean surface heat potential
h_i	Ice thickness
h_s	Snow thickness
h_{si}	Snow ice thickness
P	Snowfall rate
P_b	Rate of mechanical energy input to the mixed layer from the surface buoyancy fluxes
P_w	Rate of thermal kinetic energy input from wind stirring
P_E	Power required to entrain deep water
q_{sat}	Saturation specific humidity
q_a	Specific air humidity at 2 m
R_b	Basal melt fraction, 0.75 ($R_b = 1$ when all melt is basal)
S_b	Salinity below the mixed layer base
S_{mix}	Mixed layer salinity
S_{trap}	Effective salinity of the seawater infiltrating the submerged snow
T_a	Atmospheric temperature at 2 m
T_b	Temperature below the mixed layer base
T_f	Freezing temperature, calculated as $273.14 - 0.054S_{\text{mix}}$
T_{mix}	Mixed layer temperature
T_S^i	Snow covered ice surface temperature
T_S^o	Open water surface temperature
U_a	Wind speed at 2 m
$u_\star$	Effective friction velocity at the upper surface of the mixed layer
$u_\star^0$	Fraction velocity between the open water surface layer and mixed layer
$u_\star^i$	Friction velocity between the ice and mixed layer
$u_\star$	Effective friction velocity at the upper surface of the mixed layer
w	Entrainment rate of the mixed layer
Δb	Difference in buoyancy of the waters across the mixed layer base
δh	Thickness of snow removed during flooding (equal to the thickness of snow ice formed)

TABLE B2. Table of constants.

α	Thermal expansion coefficient, $5.82 \times 10^{-5}\,\mathrm{K}^{-1}$
β	Saline contraction coefficient, 8×10^{-4}
c_a	Specific heat capacity of air, $1005\,\mathrm{J\,kg^{-1}\,K^{-1}}$
c_w	Specific heat capacity of water, $4190\,\mathrm{J\,kg^{-1}\,K^{-1}}$
ε_s	Longwave emissivity of snow, 1
ε_w	Longwave emissivity of open water, 0.97
g	Acceleration due to gravity, $9.81\,\mathrm{m\,s^{-1}}$
k_i	Thermal conductivity of ice, $2.04\,\mathrm{W\,m^{-1}\,K^{-1}}$
k_s	Thermal conductivity of snow, $0.31\,\mathrm{W\,m^{-1}\,K^{-1}}$
L_f	Latent heat of fusion, $3.340 \times 10^6\,\mathrm{J\,kg^{-1}}$
L_s	Latent heat of sublimation, $2.834 \times 10^6\,\mathrm{J\,kg^{-1}}$
L_v	Latent heat of vaporization, $2.501 \times 10^6\,\mathrm{J\,kg^{-1}}$
p_{atm}	Atmospheric pressure, 100 kPa
ρ_a	Density of air, $1.275\,\mathrm{kg\,m^{-3}}$
ρ_i	Density of ice, $930\,\mathrm{kg\,m^{-3}}$
ρ_s	Density of snow, $400\,\mathrm{kg\,m^{-3}}$
ρ_w	Density of water, $1026\,\mathrm{kg\,m^{-3}}$
σ	Stefan Boltzmann constant, $5.67 \times 10^{-8}\,\mathrm{W\,m^{-2}\,K^{-4}}$

APPENDIX B

Variables, Constants, and Fixed Parameters

Variables, constants, and fixed parameters are given in Tables B1, B2, and B3, respectively.

TABLE B3. Table of fixed parameters.

$A_{\max}$	Prescribed maximum ice concentration, 0.95
A_{ref}	Reference ice concentration of sea ice being advected in to the domain, see Table A1
α_s	Albedo of snow, 0.8
α_w	Albedo of water, 0.06
c_1	Maximum magnitude of wind stirring in the mixed layer, 0.8
C_D^i	Turbulent transfer coefficient over ice fraction, 0.0013
C_D^o	Turbulent transfer coefficient over lead fraction, 0.001
c_h	Stanton number for mixed layer to sea ice heat transfer, 0.006
c_m	Unsteadiness coefficient, $0.03\,\mathrm{m\,s^{-1}}$
d_w	Scale depth of dissipation, 10 m
$h_{\min}$	Minimum sea ice thickness, 0.1 m
h_i^{ref}	Reference ice thickness (total) of sea ice being advected in to the domain, see Table A1
h_s^{ref}	Reference snow thickness of sea ice being advected in to the domain, see Table A1
$h_{\mathrm{si}}^{\mathrm{ref}}$	Reference snow ice thickness of sea ice being advected in to the domain, see Table A1
$I_0(0)$	Fraction of shortwave radiation that penetrates the open water surface layer, 0.45
κ_w	Extinction coefficient of shortwave solar radiation in ocean waters, $0.1\,\mathrm{m^{-1}}$
S_i	Average bulk salinity of congelation sea ice, 5
S_{si}	Average bulk salinity of snow ice, 10
R_T	Oceanic relaxation time scale, 0.25
$\tau^\star$	Relaxation time scale for advection, see Table A1

REFERENCES

Abernathey, R. P., P. I. Cerovecki, P. R. Holland, E. Newsom, M. Mazlo, and L. D. Talley, 2016: Water-mass transformation by sea ice in the upper branch of the Southern Ocean overturning. *Nat. Geosci.*, **9**, 596–601, https://doi.org/10.1038/ngeo2749.

Bintanja, R., G. J. van Oldenborgh, S. S. Drijfhout, B. Wouters, and C. A. Katsman, 2013: Important role for ocean warming and increased ice–shelf melt in Antarctic sea-ice expansion. *Nat. Geosci.*, **6**, 376–379, https://doi.org/10.1038/ngeo1767.

Bitz, C. M., P. R. Gent, R. A. Woodgate, M. M. Holland, and R. Lindsay, 2006: The influence of sea ice on ocean heat uptake in response to increasing CO_2. *J. Climate*, **19**, 2437–2450, https://doi.org/10.1175/JCLI3756.1.

Bromwich, D. H., J. P. Nicolas, and A. J. Monaghan, 2011: An assessment of precipitation changes over Antarctica and the Southern Ocean since 1989 in contemporary global reanalyses. *J. Climate*, **24**, 4189–4209, https://doi.org/10.1175/2011JCLI4074.1.

Christensen, J. H., and Coauthors, 2013: Climate phenomena and their relevance for future regional climate change. *Climate Change 2013: The Physical Science Basis*, T. F. Stocker et al., Eds., Cambridge University Press, 1217–1308.

Dee, D. P., and Coauthors, 2011: The era-interim reanalysis: Configuration and performance of the data assimilation system. *Quart. J. Roy. Meteor. Soc.*, **137**, 553–597, https://doi.org/10.1002/qj.828.

Dutrieux, P., and Coauthors, 2014: Strong sensitivity of pine island ice-shelf melting to climatic variability. *Science*, **343**, 174–178, https://doi.org/10.1126/science.1244341.

Fichefet, T., and M. A. Morales Maqueda, 1999: Modelling the influence of snow accumulation and snow–ice formation on the seasonal cycle of the Antarctic sea–ice cover. *Climate Dyn.*, **15**, 251–268, https://doi.org/10.1007/s003820050280.

Goosse, H., and V. Zunz, 2014: Decadal trends in the Antarctic sea ice extent ultimately controlled by ice–ocean feedback. *Cryosphere*, **8**, 453–470, https://doi.org/10.5194/tc-8-453-2014.

——, and Coauthors, 2018: Quantifying climate feedbacks in polar regions. *Nat. Commun.*, **9**, 1919, https://doi.org/10.1038/s41467-018-04173-0.

Gordon, A. L., 1998: Western Weddell Sea thermohaline stratification. *Ocean, Ice, and Atmosphere: Interactions at the Antarctic Continental Margin*, S. S. Jacobs and R. F. Weiss, Eds., Antarctic Research Series, Vol. 75, Amer. Geophys. Union, 215–240.

Haid, V., D. Iovino, and S. Masinna, 2017: Impacts of freshwater changes on Antarctic sea ice in an eddy–permitting sea–ice–ocean model. *Cryosphere*, **11**, 1387–1402, https://doi.org/10.5194/tc-11-1387-2017.

Haumann, F. A., N. Gruber, M. Münnuch, I. Frenger, and S. Kern, 2016: Sea-ice transport driving Southern Ocean salinity and its recent trends. *Nature*, **537**, 89–92, https://doi.org/10.1038/nature19101.

Holland, P. R., 2014: The seasonality of Antarctic sea ice trends. *Geophys. Res. Lett.*, **41**, 4230–4237, https://doi.org/10.1002/2014GL060172.

——, and R. Kwok, 2012: Wind-driven trends in Antarctic sea-ice drift. *Nat. Geosci.*, **5**, 872–875, https://doi.org/10.1038/ngeo1627.

Jacobs, S. S., H. H. Hellmer, and A. Jenkins, 1996: Antarctic ice sheet melting in the southeast pacific. *Geophys. Res. Lett.*, **23**, 957–960, https://doi.org/10.1029/96GL00723.

——, A. Jenkins, C. F. Giulivi, and P. Dutrieux, 2011: Stronger ocean circulation and increased melting under Pine Island glacier ice shelf. *Geophys. Res. Lett.*, **113**, 519–523, https://doi.org/10.1038/ngeo1188.

Jeffries, M. O., A. P. Worby, K. Morris, and W. F. Weeks, 1997: Seasonal variations in properties, and structural isotopic composition of sea ice and snow cover in the Bellinghausen

and Amundsen Seas. *J. Glaciol.*, **43**, 138–151, https://doi.org/10.1017/S0022143000002902.

——, H. R. Krouse, B. Hurst-Cushing, and T. Maksym, 2001: Snow ice accretion and snow cover depletion on Antarctic first-year sea ice floes. *Ann. Glaciol.*, **33**, 51–60, https://doi.org/10.3189/172756401781818266.

Jones, R. W., I. A. Renfrew, A. Orr, B. G. M. Webber, D. M. Holland, and M. A. Lazzara, 2016: Evaluation of four global reanalysis products using in situ observations in the Amundsen Sea Embayment, Antarctica. *J. Geophys. Res. Atmos.*, **121**, 6240–6257, https://doi.org/10.1002/2015jd024680.

Jutras, M., M. Vancoppenolle, A. Laurençoa, F. Viviera, G. Carnatc, G. Madeca, C. Rousseta, and J.-L. Tison, 2016: Thermodynamics of slush and snow–ice formation in the Antarctic sea–ice zone. *Deep-Sea Res. II*, **131**, 75–83, https://doi.org/10.1016/j.dsr2.2016.03.008.

Kirkman, C. H., and C. M. Bitz, 2011: The effect of the sea ice freshwater flux on Southern Ocean temperatures in CCSM3: Deep-ocean warming and delayed surface warming. *J. Climate*, **24**, 2224–2237, https://doi.org/10.1175/2010JCLI3625.1.

Lange, M. A., S. F. Schlosser, A. P. Ackley, P. Wadhams, and G. S. Dieckmann, 1990: ^{18}O concentrations in sea ice of the Weddell Sea, Antarctica. *J. Glaciol.*, **36**, 315–323., https://doi.org/10.3189/002214390793701291.

Lecomte, O., H. Goosse, C. Fichefet, T. de Lavergne, A. Barthélemy, and V. Zunz, 2017: Vertical ocean heat redistribution sustaining sea–ice concentration trends in the ross sea. *Nat. Commun.*, **8**, 258, https://doi.org/10.1038/s41467-017-00347-4.

Liu, J., and J. A. Curry, 2010: Accelerated warming of the southern ocean and its impacts on the hydrological cycle and sea ice. *Proc. Natl. Acad. Sci. USA*, **107**, 14 987–14 992, https://doi.org/10.1073/pnas.1003336107.

Maksym, T., S. E. Stammerjohn, S. Ackley, and R. Massom, 2012: Antarctic sea ice—A polar opposite? *Oceanography*, **25** (3), 140–150, https://doi.org/10.5670/oceanog.2012.88.

Martinson, D. G., 1990: Evolution of the southern ocean winter mixed layer and sea ice: Open ocean deepwater formation and ventilation. *J. Geophys. Res.*, **95**, 11 641–11 654, https://doi.org/10.1029/JC095iC07p11641.

Massom, R. A., and Coauthors, 2001: Snow on Antarctic sea ice. *Rev. Geophys.*, **39**, 413–445, https://doi.org/10.1029/2000RG000085.

Nicholls, K. W., L. Padman, M. Schröeder, R. A. Woodgate, A. Jenkins, and S. Østerhus, 2003: Water mass modification over the continental shelf north of Ronne Ice Shelf, Antarctica. *Geophys. Res. Lett.*, **108**, 3260, https://doi.org/10.1029/2002JC001713.

——, C. J. Pudsey, and P. Morris, 2004: Summertime water masses off the northern Larsen C Ice Shelf, Antarctica. *Geophys. Res. Lett.*, **31**, L09309, https://doi.org/10.1029/2004GL019924.

——, L. Boehme, M. Biuw, and M. A. Fedak, 2008: Wintertime ocean conditions over the southern Weddell Sea continental shelf, Antarctica. *Geophys. Res. Lett.*, **35**, L21605, https://doi.org/10.1029/2008GL035742.

——, S. Østerhus, K. Makinson, T. Gammelsrod, and E. Fahrbach, 2009: Ice-ocean processes over the continental shelf of the southern Weddell Sea, Antarctica: A review. *Rev. Geophys.*, **47**, RG3003, https://doi.org/10.1029/2007RG000250.

Parkinson, C. L., and D. J. Cavalieri, 2012: Antarctic sea ice variability and trends, 1979–2010. *Cryosphere*, **6**, 871–880, https://doi.org/10.5194/tc-6-871-2012.

Pauling, A. G., C. B. Bitz, I. J. Smith, and P. J. Langhorne, 2016: The response of the Southern Ocean and Antarctic sea ice to freshwater from ice shelves in an earth system model. *J. Climate*, **29**, 1655–1672, https://doi.org/10.1175/JCLI-D-15-0501.1.

Petty, A. A., D. L. Feltham, and P. R. Holland, 2013: Impact of atmospheric forcing on Antarctic continental shelf water masses. *J. Phys. Oceanogr.*, **43**, 920–940, https://doi.org/10.1175/JPO-D-12-0172.1.

——, P. R. Holland, and D. L. Feltham, 2014: Sea ice and the ocean mixed layer over the Antarctic shelf seas. *Cryosphere*, **8**, 761–783, https://doi.org/10.5194/tc-8-761-2014.

Pithan, F., and T. Mauritsen, 2014: Arctic amplification dominated by temperature in contemporary climate models. *Nat. Geosci.*, **7**, 181–184, https://doi.org/10.1038/ngeo2071.

Powell, D. C., T. Markus, and A. Stössel, 2005: Effects of snow depth forcing on southern ocean sea ice simulations. *J. Geophys. Res.*, **124**, C06001, https://doi.org/10.1029/2003JC002212.

Purkey, S. G., G. C. Johnson, L. D. Talley, B. M. Sloyan, S. E. Wijffels, W. Smethie, S. Mecking, and K. Katsumata, 2019: Unabated bottom water warming and freshening in the South Pacific Ocean. *J. Geophys. Res. Oceans*, **124**, 1775–1794, https://doi.org/10.1029/2018JC014775.

Renfrew, I. A., J. C. King, and T. Markus, 2002: Coastal polynyas in the southern Weddell Sea: Variability of the surface energy budget. *J. Geophys. Res.*, **107**, 3063, https://doi.org/10.1029/2000JC000720.

Schneider, D. P., and C. Deser, 2018: Tropically driven and externally forced patterns of Antarctic sea ice change: Reconciling observed and modeled trends. *Climate Dyn.*, **50**, 4599–4618, https://doi.org/10.1007/s00382-017-3893-5.

Scott, F., and D. L. Feltham, 2010: A model of the three-dimensional evolution of arctic melt ponds on first-year and multiyear sea ice. *J. Geophys. Res.*, **115**, C12064, https://doi.org/10.1029/2010JC006156.

Semtner, A. J., 1976: A model for the thermodynamic growth of sea ice in numerical investigations of climate. *J. Phys. Oceanogr.*, **6**, 379–389, https://doi.org/10.1175/1520-0485(1976)006<0379:AMFTTG>2.0.CO;2.

Shepherd, A., D. Wingham, and E. Rignot, 2004: Warm ocean is eroding west Antarctic ice sheet. *Geophys. Res. Lett.*, **31**, L23402, https://doi.org/10.1029/2004gl021106.

Stuecker, M. F., C. M. Bitz, and K. C. Armour, 2017: Conditions leading to the unprecedented low Antarctic sea ice extent during the 2016 austral spring season. *Geophys. Res. Lett.*, **44**, 9008–9019, https://doi.org/10.1002/2017GL074691.

Swart, N. C., and J. C. Fyfe, 2013: The influence of recent Antarctic ice sheet retreat on simulated sea ice area trends. *J. Climate*, **29**, 1655–1672, https://doi.org/10.1002/grl.50820.

Turner, J., T. J. Bracegirdle, T. Phillips, G. J. Marshall, and J. S. Hosking, 2013: An initial assessment of Antarctic sea ice extent in the CMIP5 models. *J. Climate*, **26**, 1473–1484, https://doi.org/10.1175/JCLI-D-12-00068.1.

——, T. Phillips, G. J. Marshall, J. S. Hosking, J. O. Pope, P. Bracegirdle, and T. J. Deb, 2017: Unprecendented springtime retreat of Antarctic sea ice in 2016. *Geophys. Res. Lett.*, **44**, 6868–6875, https://doi.org/10.1002/2017GL073656.

Walker, D. P., M. A. Brandon, A. Jenkins, J. T. Allen, J. A. Dowdeswell, and J. Evans, 2008: Oceanic heat transport onto the Amundsen Sea shelf through a submarine glacial trough. *Geophys. Res. Lett.*, **34**, L02602, https://doi.org/10.1029/2006gl028154.

Wilson, E. A., S. C. Riser, E. C. Campbell, and A. P. S. Wong, 2019: Winter upper-ocean stability and ice–ocean feedbacks in the sea ice–covered Southern Ocean *J. Phys. Oceanogr.*, **49**, 1099–1117, https://doi.org/10.1175/JPO-D-18-0184.1.

Wu, X., W. F. Budd, V. I. Lytle, and R. A. Massom, 1999: The effect of snow on Antarctic sea ice simulations in a coupled atmosphere–sea ice model. *Climate Dyn.*, **15**, 127–143, https://doi.org/10.1007/s003820050272.

Zhang, J., 2007: Increasing Antarctic sea ice under warming atmospheric and oceanic conditions. *J. Climate*, **20**, 2515–2529, https://doi.org/10.1175/JCLI4136.1.